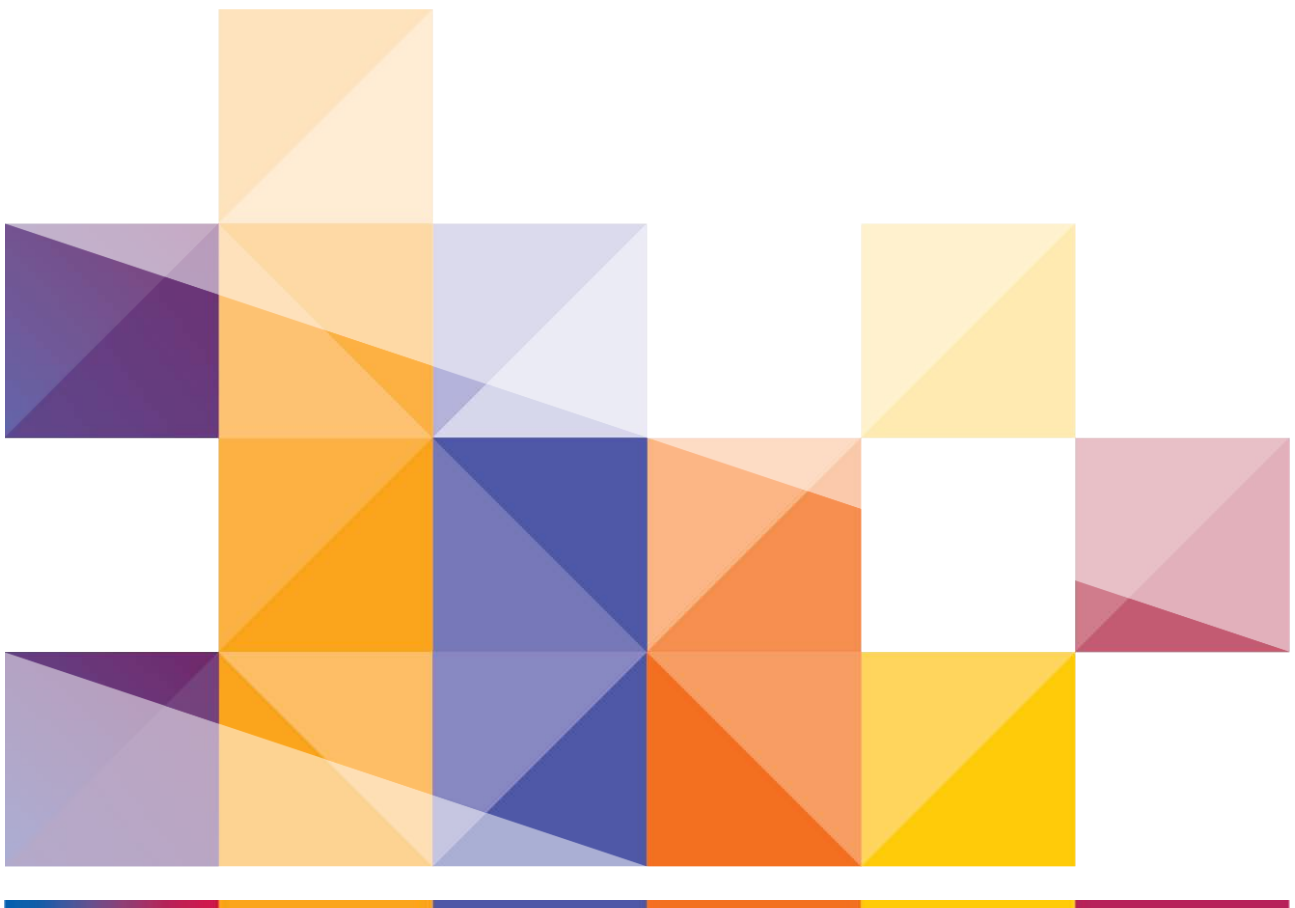


ThermoChimie

Technical report

Clay Minerals Documentation



The ThermoChimie database was first developed in 1995 by Andra, the French national radioactive waste management agency. They have since been joined by Radioactive Waste Management (RWM) from the UK, and ONDRAF/NIRAS from Belgium.

ThermoChimie provides an accurate and consistent set of data specifically chosen for use in modelling the behaviour of radionuclides in waste packages, engineered barriers, and both the near surface and deep geosphere. The database can be used to model the speciation and solubility of a wide range of stable and radioactive elements, organics, and solid phases including cements, clay minerals and degradation products (such as zeolites). The database is suitable for use within the range of conditions expected in both near-surface and geological disposal facilities: pH 6-14, ionic strength up to 5M, Eh within the stability fields of water, and temperatures from 15 to 80°C.

ThermoChimie is intended for use across the radioactive waste management community, to support repository performance assessment, research and development activities and decision making. To maximise their utility the data are therefore provided in formats suitable for use with common geochemical modelling codes. The database can be viewed and downloaded from the project website: <https://www.thermochimie-tdb.com/>, where additional information and supporting documents are also available.

In numerous deep disposal nuclear waste concepts, clay minerals are important constituents of the system, from the engineered to the geological barrier. Thermodynamic properties of clay minerals, as reactive components of clayrock, are necessary for the understanding and quantification of water-rock interactions in/around a deep disposal (Culois-Oxfordian). General modeling purposes require stability constants of the initial clay composition, to provide a first geochemical framework. In addition, the chemical disturbances (alkaline interactions) may imply transformations among the initial minerals, which supposes to obtain the thermodynamic properties for a large number of clay mineral potential end members. Indeed, many experiments have been performed in the past, concerning the long term behavior of clay materials, indicating that strong transformations are influenced by the alkaline solutions issued from the cementitious materials (Gaucher and Blanc, 2006). Interactions in iron rich media or induced by glass dissolution may also lead to strong transformation of structure and the composition of clay minerals. It is thus of importance to provide thermodynamic properties for end members that could potentially form, according to the physico-chemical conditions.

The document presents the strategy and the results obtained, throughout the ThermoChimie programs, concerning the clay minerals thermodynamics properties. This implies a large panel of clay systems of which properties have been obtained or selected in a consistent way: 10 Å phases (smectites, illites), 14 Å phase (chlorites) and 7 Å phases (kaolinite, berthierine, ...).

The strategy applied in this work implies, from a limited number of measurements, to extend the results to different compositions, by using predictive models. Models are then parameterized using measured data from both the literature and dedicated experiments.

The document is then presenting:

- The experimental measurements performed on selected minerals
- A selection for the minerals whose properties had been measured
- The predictive models, based on previous selection and measurements
- A database for theoretical clay minerals end members, of which properties are calculated using the models developed here.



1. Clay mineral Structure

Clay minerals belong to the largest family of phyllosilicates, which means that their crystalline cell basically consists in stacking sequences of layers based on silicates and oxide/hydroxides sheets. For example illite, a 10 Å (distance between two layers) phyllosilicate, displays layers formed by two silicates sheets that enclose a third octahedral sheet (TOT sheet, see Figure 1). Between two layers, alkaline or earth alkaline cations compensate the unbalanced, negative charge. The interlayer cations may be anhydrous, like in illite, or hydrated, as in the case of smectites or vermiculites. For 7 Å phases, the interlayer space is empty whereas it contains an additional octahedral (brucitic) sheet for 14 Å mineral (case of chlorites).

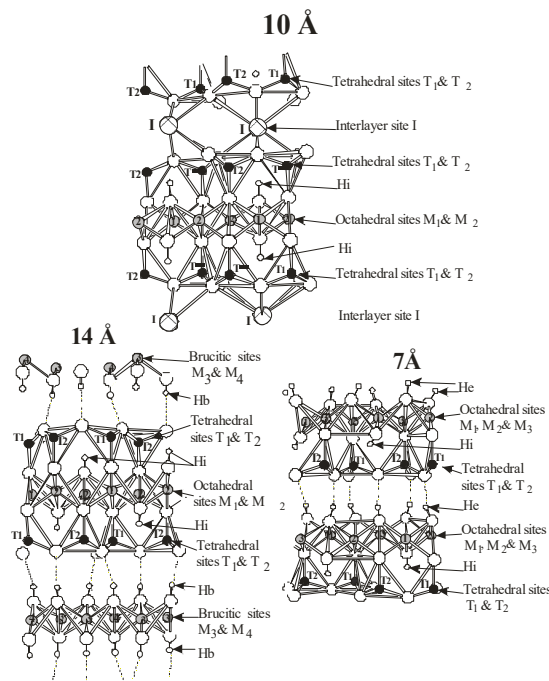


Figure 1 - Crystal structures of 10Å, 14Å and 7Å phyllosilicates showing the positions of different crystallographic sites.

Considering the thermodynamic properties of phyllosilicates, data are available for micas and for phases with a structure close to that of talc, kaolinite and for chlorites, to a lesser extent. On the other hand, thermodynamic properties are lacking for phases such as smectites, vermiculite or illite. Several Gibbs energies of formation ΔG°_f have been indirectly measured from aqueous solubility experiments (numerous examples in Vieillard (2000)). This is the reason why, for phases that belong to those families, the thermodynamic properties have been acquired within the frame work of the Thermochimie project.

2. Recent advances

Until now, much of the available thermodynamic data for clay minerals have been derived either from solution experiments or from predictive calculations. Numerous experimental studies of equilibration in solution have been conducted since the pioneering work of Reesman and Keller (1968). Equilibration experiments on illite were repeated by Kittrick (1984) and Aja et al. (1991). The case of smectite was investigated, among others, by Reesman and Keller (1968), May et al. (1986), and Kittrick and Peryea (1988). Essene and Peacor (1995) criticised the solution experiments and the properties derived from these studies have not been included so far in the usual thermodynamic databases for geochemical modelling. To overcome such issues, calorimetric measurements have been carried out in the last decade, on a variety of clay minerals, following methods which are described in detail by Gailhanou et al. (2007, 2009, 2012 and 2013) and Blanc et al. (2014). A compilation of the measured thermodynamic properties is provided by Blanc et al. (2015). Recently, Gaboreau et al. (2020) showed, for four clay mineral samples, that solution experiments could provide thermodynamic properties close to calorimetric measurements. This result was achieved under the following conditions: (i) equilibration experiments lasting at least two (2) years, and (ii) reaction temperature increasing from 25 to 40°C, to enhance equilibration kinetics. Note that both calorimetry and solubility experiments were performed on the same samples.

For decades, estimation methods (Chermak and Rimstidt, 1989; Van Hinsberg et al., 2005a, b; Vieillard, 2000, 2002) remained the usual source of thermodynamic data for clay minerals, although neither parametrization nor verification could be assessed against the thermodynamic properties of actual clay minerals. Blanc et al. (2015) proposed a model, based on Vieillard and Tardy (1988), Vieillard (1994a), Vieillard (1994b) and on Chermak and Rimstidt (1989) formalisms to estimate the whole set of thermodynamic properties ($\Delta_f H^0$, S^0 , $C_p^0(T)$ and even V^0). The model was parameterized and verified, on the basis of properties extracted from calorimetric measurements performed on actual clay minerals. Unfortunately, the model by Blanc et al. (2015) only applies to anhydrous phases, and it cannot be verified with respect to the experimental data and the compilation of solubility constants recently provided by Gaboreau et al. (2020).

To overcome this difficulty, H₂O vapour isotherms were measured by Gailhanou et al. (2017) and Vieillard et al. (2019), and the results were gathered to develop a hydration model able to predict thermodynamic properties of hydration over a large range of clay mineral compositions. Combining the approaches developed by Blanc et al. (2015), Gailhanou et al. (2017) and Vieillard et al. (2019) would allow the prediction capacities to be tested with respect to solubility data obtained or selected by Gaboreau et al. (2020). A similar approach was proposed by Vidal and Dubacq (2009) and Dubacq et al. (2010). In our case, parameterization and verification are performed based on thermodynamic properties measured directly on clay minerals.

The approaches developed by Blanc et al. (2015), Gailhanou et al. (2017) and Vieillard et al. (2019) can be combined according to the workflow displayed in Figure 2. Ultimately, it allows equilibrium constants to be predicted for clay minerals and a comparison of the calculated thermodynamic properties to be made with respect to solubility data selected from the literature.

3. Theoretical background

Classic thermodynamic relations and conventions theoretically apply to clay minerals as with any other mineral. Consequently, the formation properties of a clay mineral will depend on the definition of a reference state. The reference state is considered as the standard state, at 1 bar and 298.15K. Following Helgeson et al. (1978), the pressure between the temperature interval 273.15 to 373.15K is constant, at 1 bar. For $T > 373.15\text{K}$ (100°C), the pressure is obtained from the water liquid-vapour curve. Considering a phase AB, its apparent Gibbs free energy of formation $\Delta_a G_{AB,P,T}^0$ is given, at P and T, by the relation:

$$\begin{aligned} \Delta_a G_{AB,P,T}^0 &= \Delta_f H_{AB,P,T}^0 - T \cdot S_{AB,P,T}^0 \\ &= \Delta_f H_{AB,P_r,T_r}^0 - T \cdot S_{AB,P_r,T_r}^0 + \int_{T_r}^T C_{p,AB}^0 dT - T \cdot \int_{T_r}^T \frac{C_{p,AB}^0}{T} dT + \int_{P_r}^P V_{AB}^0 dP \end{aligned} \quad \text{Eq. 1}$$

where T_r : temperature at the reference state (298.15 K); P_r : pressure at the reference state (0.1 MPa); $\Delta_f H_{AB,P,T}^0$: enthalpy of formation of the phase AB at temperature T and pressure P; $S_{AB,P,T}^0$: the third law entropy of the AB phase; $C_{p,AB}^0$: heat capacity of the AB phase; V_{AB}^0 : molar volume of the AB phase, independently of temperature.

This definition follows the Benson–Helgeson convention (Benson, 1968; Helgeson et al., 1978) where $\Delta_a G_{AB,P,T}^0$ equals $\Delta_f G_{AB,P,T}^0$ only at 25°C . The heat capacity function is related to the dependence of entropy and formation enthalpy with temperature through:

$$\Delta_a H_{AB,P,T}^0 = \Delta_f H_{AB,T_r}^0 + \int_{T_r}^T C_{p,AB}^0 dT \quad \text{and} \quad S_{AB,P,T}^0 = S_{AB,T_r}^0 + \int_{T_r}^T \frac{C_{p,AB}^0}{T} dT \quad \text{Eq. 2}$$

The third law entropy term, at T_r , includes the heat capacity function, and a residual contribution:

$$S_{AB,P_r,T_r}^0 = \int_0^{T_r} \frac{C_{p,AB}^0}{T} dT + S_{AB}^{\text{mag}} + S_{AB}^{\text{conf}} \quad \text{where} \quad \int_0^{T_r} \frac{C_{p,AB}^0}{T} dT = S_{AB,P_r,T_r}^{\text{lat}} \quad \text{Eq. 3}$$

with $S_{AB,P_r,T_r}^{\text{lat}}$ standing for the lattice entropy. The two first terms in Equation (3) can be measured by low temperature calorimetry (PPMS or adiabatic calorimetry, Gailhanou et al. (2012)) and S_{AB}^{mag} represents the magnetic entropy (Holland, 1989a). For the configuration entropy term S_{AB}^{conf} , Ulbrich and Waldbaum (1976) proposed a calculation method for assessing the maximum value of both the magnetic and the configurational entropy terms. For the S_{AB}^{conf} term, the method is based on a site mixing approach and for the magnetic contribution, on the maximum number of spin configurations according to:

$$S_{AB}^{\text{mag}} = R \sum_i x_i^{AB} \ln(2S_i + 1) \quad \text{Eq. 4}$$

where R is the gas constant, x_i^{AB} the amount of element i in solid AB, and S_i its spin number. This expression is valid for the metals of the first transition series for which the valence electrons are in the outermost shells.

The illite/smectite case needs to define solid solution properties. Considering a second solid phase CB, its Gibbs free energy $\Delta_f G_{SS,P,T}^0$ results from the combination of both end-members' Gibbs free energy, $\Delta_f G_{AB,P,T}^0$ and $\Delta_f G_{CB,P,T}^0$ by :

$$\Delta_f G_{SS,P,T}^0 = x \cdot \Delta_f G_{AB,P,T}^0 + (1 - x) \Delta_f G_{CB,P,T}^0 + \Delta G_{SS,P,T}^{\text{mix}} \quad \text{Eq. 5}$$

Where x and $\Delta G_{SS,P,T}^{\text{mix}}$ correspond respectively to the fraction of AB end-member and the Gibbs energy of mixing. The latter can be decomposed into enthalpy $\Delta H_{SS,P,T}^{\text{mix}}$ and entropy $\Delta S_{SS,P,T}^{\text{mix}}$ of mixing terms:

$$\Delta G_{SS,P,T}^{\text{mix}} = \Delta H_{SS,P,T}^{\text{mix}} - T \cdot \Delta S_{SS,P,T}^{\text{mix}} \quad \text{Eq. 6}$$

The entropy of mixing can be estimated, at first approximation, considering an ideal mixing between end-members, resulting in:

$$\Delta S_{SS,P,T}^{\text{mix}} = -R \cdot [x \ln(x) + (1 - x) \ln(1 - x)] \quad \text{Eq. 7}$$

As for the equilibrium of AB in an aqueous solution, we consider the dissolved species A^+ and B^- and the chemical reaction:



Any reaction property $\Delta_r \Xi_{AB,P,T}^0$ can be obtained from the corresponding formation property $\Delta_f \Xi_{AB,P,T}^0$, according to the relation:

$$\Delta_r \Xi_{AB,P,T}^0 = \Delta_f \Xi_{A^+,P,T}^0 + \Delta_f \Xi_{B^-,P,T}^0 - \Delta_f \Xi_{AB,P,T}^0 \quad \text{Eq. 9}$$

where Ξ stands for G, H or S, or any other property. Finally, the Gibbs free energy of reaction (3) is related to the equilibrium constant of the reaction, $K_{AB,P,T}$, by:

$$\Delta_r G_{AB,P,T}^0 = -R \cdot T \cdot \text{Log} K_{AB,P,T} \cdot \ln(10) \quad \text{Eq. 10}$$

$$\Delta_r G_{AB,P,T}^0 = -R \cdot T \cdot \log_{10} K_{AB,P,T} \cdot \ln(10)$$

Clay minerals may undergo hydration reactions (smectites and vermiculites). In more detail (Gailhanou et al., 2017), a hydration reaction may be expressed by:



We can consider the property of hydration $\Delta \Xi_{\text{hyd},Tr}^0$ (per H_2O mole) for a given clay mineral having n bounded molecules per half-cell. It is related to the total formation property $\Delta \Xi_{f,Tr}^0$ of the mineral through the following relation:

$$\Delta_f \Xi_{Pr,Tr}^0(\text{hydrated clay}) = \Delta_f \Xi_{Pr,Tr}^0(\text{anhydrous clay}) + n_{\text{H}_2\text{O}} \cdot \Delta_f \Xi_{Pr,Tr}^0(\text{H}_2\text{O}) + n_{\text{H}_2\text{O}} \cdot \Delta_{\text{hyd}} \Xi_{Pr,Tr}^0 \quad \text{Eq. 12}$$

where $\Delta_f \Xi_{Pr,Tr}^0(\text{hydrated clay})$, $\Delta_f \Xi_{Pr,Tr}^0(\text{dehydrated clay})$ and $\Delta_f \Xi_{Pr,Tr}^0(\text{H}_2\text{O})$ stand for the formation property for the hydrated mineral, the dehydrated mineral and the bulk water, respectively. The scheme followed to calculate thermodynamic properties for hydrated clay minerals is illustrated in Figure 2. In that figure, the properties of formation for an hydrated phase are deduced from the properties of formation of the anhydrous phase adding the properties of hydration. The properties of bulk water are supposed to be known. The scheme implies avoiding to consider directly the properties of formation of the hydrated phase and, rather, to split the studies into the anhydrous phase and the properties of hydration. This choice

arises especially because of the difficulty to maintain a stable hydration state close to $P/P_0 = 1$ (Gailhanou et al., 2012), throughout the whole measurement process.

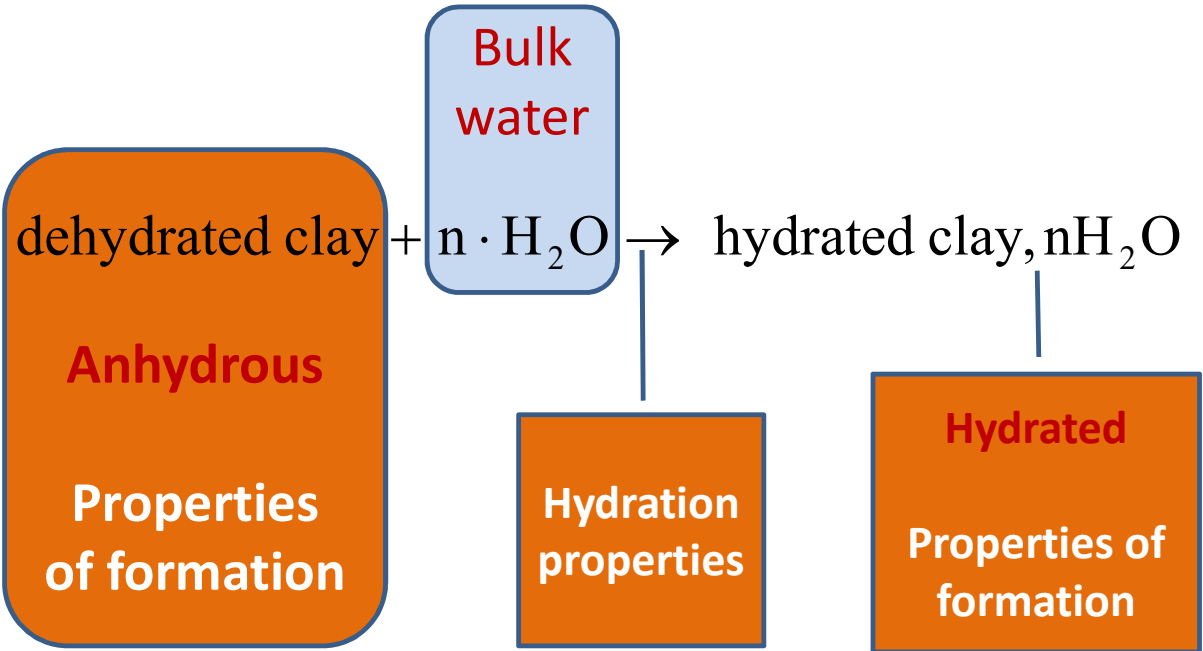


Figure 2 - Reaction scheme for studying the thermodynamic properties of hydrated minerals.

4. Experimental methods for clay minerals thermodynamic properties measurements

According to the scheme displayed in Figure 2 the measurement of thermodynamic properties for clay minerals is splitted into 1) measurement of formation properties for anhydrous minerals and 2) to combine with measured hydration reaction properties.

4.1. MEASURING THERMODYNAMIC PROPERTIES FOR ANHYDROUS CLAY MINERALS

4.1.1. General aspects

The complete thermodynamic dataset of a clay mineral (ΔH_f^0 , ΔG_f^0 , C_{pTr} , S^0), at 1 bar and a wide range of temperature, can be determined by calorimetry. This implies the use of several calorimetric techniques, which are listed, below. First, some preliminary points must be underlined:

- In most cases, a natural or synthetic clay sample contains impurities, despite physico-chemical treatments carried out for purifying the samples,
- For calorimetric experiments, determining the nature, the chemical composition and the amount of impurities is crucial for assessing the feasibility of measurements on a sample.
- Those impurities have to be well characterized and their thermodynamic properties, well known because the contribution of impurities has to be subtracted.

Table 1 summarizes the different techniques that have been implemented in order to get a full set of thermodynamic parameter for a given anhydrous clay mineral. A detailed description of each technique is provided in the following sections.

Table 1 - Summary of the calorimetric techniques implemented in the measurements.

CALORIMETRIC TECHNIQUES	MEASURED PROPERTIES	THERMODYNAMIC FUNCTIONS	
Isothermal dissolution calorimetry (IM2NP, Marseille)	Enthalpies of dissolution $\Delta H_{diss,298}^{\circ}$	Standard enthalpies of formation $\Delta H_f^{\circ}, 298$	Enthalpies of formation $\Delta H_f^{\circ}(T)$ Entropies $S^{\circ}(T)$ Gibbs free energies of formation $\Delta G_f^{\circ}(T)$
Low-temperature adiabatic calorimetry (5 – 380K) (Utrecht, Netherlands ;Tsukuba Univ., Japan ;TokyoTech, Japan) PPMS calorimetry (TokyoTech, Japan) DSC (300 K – 500 K) (IM2NP, Marseille)	Low temperature heat capacities $C_p^{\circ}(T)$	Entropies $S^{\circ}(T)$ Heat contents $H^{\circ}_T - H^{\circ}_{298}$	
Volumetric or gravimetric adsorption isotherm + calorimetric measurements (Mons, Belgique;LCP, Marseille)	Amounts of adsorbed water and Heats of adsorption(*) vs. RH	Enthalpies(*) and Gibbs free energies of hydration vs. RH	

4.1.2. Enthalpy of formation

The standard enthalpy of formation of a clay mineral is obtained indirectly from reaction-solution calorimetry. Two methods may be implemented, acid solution calorimetry at low temperature (room temperature or less than 100°C) and drop solution calorimetry at high temperature (close to 700°C for lead borate) in molten oxides. For both methods, apparatuses are Tian-Calvet heat-flux microcalorimeters (Ganteaume et al., 1991; Navrotsky, 1997). In this document, we will discuss only the acid solution calorimetry which is the method used for measurements on clay minerals.

For solution calorimetry at 298.15 K, the method implements several reactions of dissolution of (i) clay sample (= clay mineral + impurities), (ii) formative constituents of the clay mineral in appropriate stoichiometry and (iii) impurities present in the clay sample. An appropriate combination of these reactions leads to the reaction of formation of the clay mineral from its formative constituents at 298.15 K and 1 bar. The acid solution is generally a hydrofluoric and nitric acid solution, with a composition optimized to dissolve totally the clay samples and the formative constituents in a reasonable time (a few hours). Formative constituents, which contain elements constitutive of the clay mineral, are generally oxides or hydroxides, and may be also nitrates and fluorides (Gailhanou et al., 2012). To dissolve a mixture of formative constituents and impurities rather than each phase independently, allows minimizing the uncertainty associated with the enthalpy of formation of the clay mineral. An example of application of this method is given for an illite further on.

4.1.3. Heat capacity

The heat capacity of a clay mineral may be measured for a very wide range of temperatures, from 2 K to 1000 K, using several complementary techniques. Among available techniques, adiabatic calorimetry is especially suitable for measuring heat capacities at low temperature. Low temperature adiabatic calorimetry (low-TAC) is commonly used and allows Cp measurements from 10 - 15 K to about 350 K (Gailhanou et al., 2009; Gailhanou et al., 2007). It requires an important amount of sample (about 10 g) to optimize the Cp contribution of the sample compared to that of the cell, especially at low temperature. This technique presents a very good accuracy on the measurements, assessed using a standard reference material, with deviations on Cp values generally lower than 0.1% above 100 K. The relative uncertainties (scattering) of the Cp measurements have been estimated on three clay minerals to be lower than 0.3% between 150 K and 350 K (Gailhanou et al., 2007).

Recently, a heat-pulse calorimeter has been commercialized by Quantum Design® and allows measuring heat capacities of minerals at low temperatures (heat capacity option of the Physical Properties Measurement System (PPMS)). One of the main differences with low-TAC is the amount of sample, as only a few milligrams are necessary for PPMS measurements. Consequently, a high purity and homogeneity of the sample are required for the measurement to be representative of the whole sample. The reliability of this technique has been assessed by Dachs and Bertoldi (2005) for three synthetic minerals, between 5 K and 300 K. Thus, Dachs and Bertoldi (2005) obtained relative errors lower than 0.5% between 100 and 300 K for single-crystal and sintered-powder samples and underestimated of about 1-2% the Cp of sealed powder samples. The relative uncertainties (scattering) were estimated to be, at best, lower than 0.3% for $T > 50$ K.

A third complementary technique, commonly used for higher temperatures, is differential scanning calorimetry (DSC). Using this technique, heat capacities of clay samples may be measured from 143 K to high temperatures. The amount of sample is about a few hundreds of milligrams. Standard deviations on Cp values are lower than 1% at $T > 200$ K (Gailhanou et al., 2007, 2009). For clay minerals, they are strong limits to this technique:

- the highest temperature, for anhydrous clay minerals, are reached when deshydroxylation begins (depending on the mineral, from 300 to 600°C);
- for hydrated phases, this technique is difficult to apply since the loss of water may start close to room temperature.

Afterwards, heat capacities of the mineral $C_{p, \text{miner}}$ are determined by subtracting the contribution of impurities, according to a relation based on an additivity law:

$$C_{p, \text{miner}} = \frac{C_{p, \text{sample}} - \sum_i X_i C_{p, i}}{X_{\text{miner}}} \quad \text{Eq. 13}$$

where X_{miner} is the mass fraction of the mineral, $C_{p, \text{sample}}$ is the heat capacity of the sample, X_i is the mass fraction of impurity i and $C_{p, i}$ is the heat capacity of impurity i (in $\text{J}\cdot\text{g}^{-1}\cdot\text{K}^{-1}$).

4.1.4. Residual entropy

A part of the total entropy of a mineral cannot be measured. It is called residual and, for clay minerals, it originates from two main sources: the configurational and the magnetic entropy.

Configurational entropy

It is associated to the disorder that occurs when mixing different cations in the same crystallographical site (octahedral, tetrahedral and interlayer sites). This entropic term is not negligible in the case of clay mineral, but its determination requires specific analyses and structural modeling. Usually it is estimated to its maximum value using Ulbrich and Waldbaum (1976) method. However several investigations have been done to improve the knowledge of cationic distribution in the different crystallographic sites of clay minerals, based on spectroscopic analyses (^{29}Si NMR, ^{27}Al NMR) and mechanistic calculations (Cuadros et al., 1999; Sainz-Díaz et al., 2001; Sainz-Díaz et al., 2003) or X-ray diffraction (Drits et al., 2006). Until now, these studies concern mainly illites, smectites and interstratified illite-smectites. Some studies are trying to generalize such measurements, like the model of Vinograd (1995) for the tetrahedral sites of layered silicates.

Magnetic entropy

In the case of clay minerals containing paramagnetic elements (generally Fe, Mn), a magnetic transition, associated with the order/disorder transition of magnetic spins of paramagnetic ions, may appear and generate an anomaly on the C_p curve, at very low temperatures (Ulbrich and Waldbaum, 1976). For instance, for iron-rich chlorites (chamosite), magnetic transition occurs at temperatures lower than 7 K (Townsend et al., 1986). Magnetic entropy can be included in the calorimetric entropy when C_p is measured starting from those very low temperatures. In most cases, when magnetic transition happens, it concerns only a part of the paramagnetic ions, so that the calculation of maximum magnetic entropy according to Ulbrich and Waldbaum (1976) formula $S_{\text{spin}}^0 = R \sum_i x_i \ln(2s_i + 1)$, with x_i the molar fraction and s_i the spin quantum number of paramagnetic ion i in the clay mineral, leads to an overestimation (Gailhanou et al., 2009).

4.2. EXPERIMENTAL MEASUREMENTS OF HYDRATION PROPERTIES

4.2.1. Devices and methodology

The devices for experimental measurement of hydration properties are listed in Table 1. It implies the use of volumetric or gravimetric water adsorption apparatuses. Gailhanou et al. (2017) have provided a methodology to extract the properties from 2 isotherms acquired at 2 different temperatures. An alternative path could be to use 1 isotherm and the measurement of the heat release during hydration using a calorimeter. The latter method is not developed here since its enforcing implies calibration issues which could not be solved during the course of the different Thermochimie projects.

4.2.2. Extracting raw hydration properties from water vapor isotherms at 2 different temperatures

The methodology used in the Thermochimie project to extract the hydration properties from 2 water adsorption isotherms at 2 different temperatures had been fully described by Gailhanou et al. (2017) for the Na-saturated MX-80 smectite and only a brief summary is given here. The method relies on the discrimination of two main types of water contributing to the total amount of water absorbed in a powder clay sample used for such measurements: one directly associated to the clay, called “clay water” and the other one depending on the microtexture of the sample, referred as “capillary water”. As described in Gailhanou et al. (2017), the “clay water” refers to interlayer water and water hydrating cations on external clay surfaces (i.e. strongly influenced by cations), whereas the “capillary water” refers to water filling the pore spaces and multilayer water on external surfaces low influenced by compensating cations. The method developed by the group of authors supposes two mains steps, that is:

- (i) to discriminate in the water adsorption isotherms, the amounts of clay water and capillary water, respectively;
- (ii) to use a thermodynamic approach to extract from the experimental isotherms, the energies of formation of the clay water (G, H, S).

The removal of capillary water and the extraction of the thermodynamic properties uses a specific mathematical formalism. It starts by first considering the reaction where water vapor (superscript g) is adsorbed onto dried clay at P:



The Gibbs free energy of the adsorption reaction ($\Delta_{\text{ads}}G_{T,P}$) can be calculated according to the following expression :

$$\Delta_{\text{ads}}G_{T,P} = \int_0^n (\mu_{a,T,P} - \mu_{w,T,Pr}^0) \cdot dn = RT \cdot \int_0^n \ln\left(\frac{P}{P_s}\right) \cdot dn \quad \text{Eq. 15}$$

where P_s is the saturation water vapor pressure at T .

According to this latter equation, $\Delta_{\text{ads}}G_{T,P}$ can be determined by plotting $RT \cdot \ln(P/P_s)$ against the water content n and by calculating the area under the curve from $n = 0$.

The enthalpy and entropy of adsorption (ΔH_{ads} and ΔS_{ads}) may then be derived by considering isotherms at two temperatures, T_1 and T_2 , using an adaptation of the Clausius-Clapeyron's equation (Hill, 1949, 1950). The determination of these properties is described in Gailhanou et

al. (2017). In the previous equations, the amounts of water were non-specifically designated as n . Considering the subscript “ads”, “cap” and “C.W” for the respective contributions of the total adsorbed water, the capillary water and the clay water, the total amount of water n can be expressed as:

$$n = n_{\text{ads}} = n_{\text{cap}} + n_{\text{C.W}} \quad \text{Eq. 16}$$

In order to discriminate the clay water and the capillary water in the adsorption isotherms, a method was developed in Gailhanou et al. (2017) based on the combination of adsorption isotherm with structural data obtained from previous XRD analyses and modeling studies (Cases et al. 1992, 1997, Berend et al. 1995, Ferrage et al. 2005). An empirical relationship was then proposed allowing to estimate the amount of capillary water from the square of the total amount of adsorbed water, which is:

$$N_{\text{cap.}} = B * (n_{\text{ads}})^2 \quad \text{Eq. 17}$$

where B is a fitting coefficient defining the sharing between the two types of water. This parameter may be determined from at least one measurement for the whole RH domain. From (Eq-2) and (Eq-3), it comes:

$$n_{\text{C.W}} = n_{\text{ads}} (1 - B * n_{\text{ads}}) \quad \text{Eq. 18}$$

The removal of capillary water is processed using equation Eq. 18, in the interval 30-100% RH, as capillary water doesn't exist at lower RH values (Lassin et al., 2005). In addition, the formation properties of clay water $\Delta G_{\text{f}}(\text{H}_2\text{O})_{\text{C.W}}$, $\Delta H_{\text{f}}(\text{H}_2\text{O})_{\text{C.W}}$ and $\Delta S(\text{H}_2\text{O})_{\text{C.W}}$ are calculated using the relationships established in Gailhanou et al. (2017), expressed by:

$$n_{\text{ads}} \Delta \Xi_{\text{f}}(\text{H}_2\text{O})_{\text{ads}} = n_{\text{C.W}} \cdot \Delta \Xi_{\text{f}}(\text{H}_2\text{O})_{\text{C.W}} + n_{\text{cap}} \cdot \Delta \Xi_{\text{f}}^0(\text{H}_2\text{O})_{\text{cap}} \quad \text{Eq. 19}$$

where Ξ refers to G, H or S. Parameters n_{ads} , n_{cap} , $n_{\text{C.W}}$ and $\Delta G_{\text{f}}(\text{H}_2\text{O})_{\text{ads}}$, $\Delta H_{\text{f}}(\text{H}_2\text{O})_{\text{ads}}$ and $\Delta S(\text{H}_2\text{O})_{\text{ads}}$ have been determined previously from water adsorption isotherms at two temperatures. The thermodynamic properties of capillary can be computed using the Thermo-ZNS calculation code (Gailhanou et al., 2017; Lassin et al., 2005, 2016).

5. Critical selection from the literature

A critical selection of phyllosilicates and related phase has been performed first, in order to provide consistent thermodynamic properties for some phases of interest within a deep disposal context and second, in order to provide more accurate and traceable data for predicting models. We are giving here one example of selection (for kaolinite), in order to explain the process leading to the thermodynamic data selection from a literature review. Thereafter, the properties gathered for the other phases are reported.

5.1. SELECTION GUIDELINES

The selection is focused on the collection of direct and traceable measurements. In addition, internal calculations are performed by using the properties of elements and aqueous species already selected within the framework of the Thermochemie project. The selection is using the following guidelines:

- when possible, we avoid using solution equilibrium experiments, which could lead to misleading results because of the difficulty to reach equilibrium state with clay minerals, because of kinetic issues,

- when possible, LogK(T) function are calculated using calorimetric data and compared to the results of solution equilibria in order to get a verification involving different experimental techniques,

- solution equilibria results are selected according to the electroneutrality condition, the duration of the experiment, the analysis of final solid products and the experimental protocol,

- equilibrium constants extracted from solution equilibria are recalculated by using the Thermochemie Database ,

- the selection is finally verified by drawing activity diagrams involving the minerals of interest in the chemical sub systems of concern, to ensure phase relations are consistent with mineralogical observations from the literature.

5.2. EXAMPLE OF MINERAL SELECTION: THE CASE OF KAOLINITE, $Al_2Si_2O_5(OH)_4$

Kaolinite is the most widespread 7 A phyllosilicate. This case is particularly suitable to illustrate the literature review process since a lot of calorimetric measurements have been performed on this mineral. In addition, it had been used into solution experiments at various temperatures, which allows verifying the parameters selected.

5.2.1. Selection of the thermodynamic constants

For the enthalpy of formation, the following studies could be gathered:

- Hemingway et al. (1978), -4120.10 kJ/mol, (HF dissolution calorimetry)

- De Ligny and Navrotsky (1999), -4120.20 kJ/mol (high temperature lead borate calorimetry)
- Fialips et al. (2001), -4115.30 kJ/mol (high temperature lead borate calorimetry)

The first value is corrected from an older experiment (Barany and Kelley, 1961), for a sample containing impurities. The sample used by De Ligny and Navrotsky (1999) also contains accessory minerals whose contribution to the total enthalpy ranges, according to the authors, between 6 et 22kJ per mole of kaolinite. In order to avoid impurities, Fialips et al. (2001) have synthesized 6 kaolinites, following 6 different processes. All their measurements fall within the same error interval, ± 4.1 kJ/mol. We have selected the measurements performed by Fialips et al. (2001).

For entropy direct measurement, different authors have used the adiabatic calorimetry:

- King and Weller (1961), 202.92 J/mol.K, acquired from 50 to 300K
- Hemingway et al. (1978), 203.70 J/mol.K (corrected from the previous authors)
- Lipsicas (1986) et al., 183.15 J/mol.K, acquired from 110 to 300K
- Robie and Hemingway (1991), 200.90 J/mol.K, acquired from 20 to 380K.

After Robie and Hemingway (1991), Lipsicas et al. (1986) would have made errors in calibrating their apparatus. In addition, it appears that the measurement from Robie and Hemingway (1991) have been performed over the largest temperature interval, especially concerning the lower temperatures limit. It must be noted that between 0 K and the first measured temperature, the values are always approximated by calculation. According to the selection criteria, we thus retain the experiment from Robie and Hemingway (1991) which are less dependent on calculation results. In addition, we are selecting the $C_p^\circ(T)$ function acquired by these authors for sake of consistency with the S°_{298} selection and because no other measurements are available (to our knowledge). Combining selected $\Delta H^\circ_{f,298}$ and S°_{298} and using the elements entropy from Thermochemie database provides a $\Delta G^\circ_{f,298}$ of -3793.94 kJ/mol.

5.2.2. Verification of the selection using solution equilibria experiments

The verification is realized by comparing the $\text{Log}K(T)$ function calculated from the previously selected thermodynamic parameters with experimental results from solution equilibria experiments, collected from the literature and displayed in Figure 3. All the equilibrium constant are issued from experimental studies, expected for Helgeson et al. (1978) whose equilibrium constant is calculated from field observations and analyses. In addition, it must be noted that no fitting procedure is involved for the $\text{Log}K(T)$ function. Indeed, the function calculated by using aqueous complexes from Thermochemie and the thermodynamic properties selected previously is consistent with results from equilibrated solutions. Except for one point, the spread of the solubility values at 25°C is not worse than what is observed at higher temperature, implying that temperature alone (and thus kinetic factors) cannot be the only explanation for this scattering.

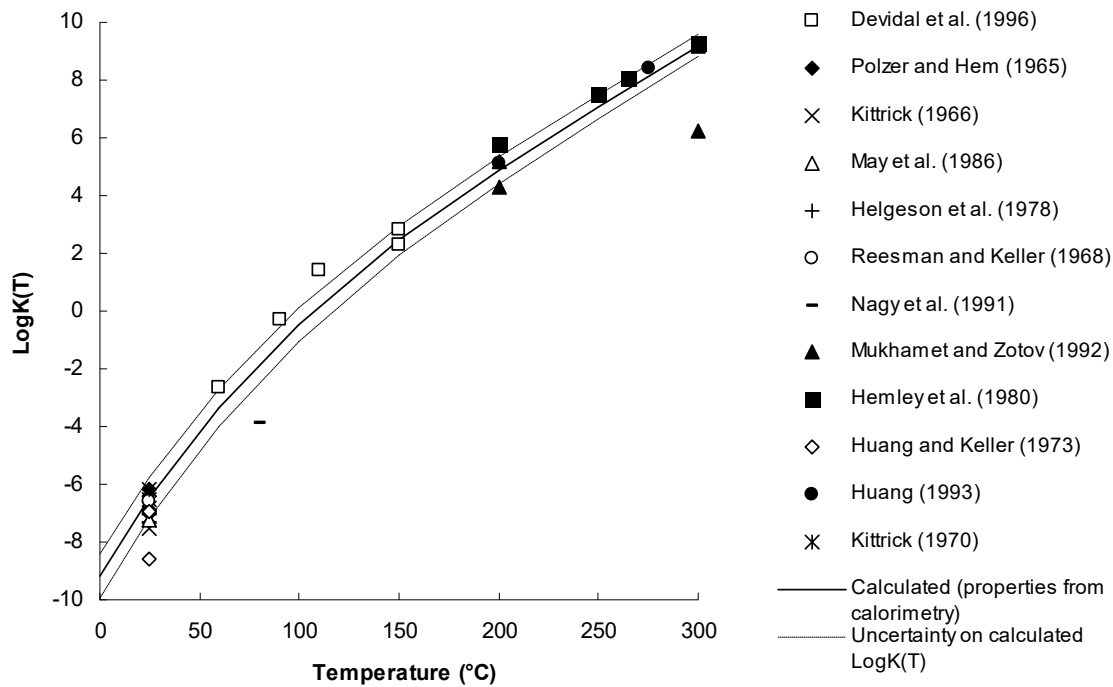


Figure 3 - Kaolinite equilibrium constant as a function of temperature.

5.3. PROPERTIES SELECTED

Full sets of thermodynamic data are available for the following phases: talc, pyrophyllite, muscovite, phlogopite, paragonite, margarite, lizardite, kaolinite and fibrous minerals (chrysotile). In addition, Holland and Powell (1998) and Vidal et al. (2005) did produced data concerning chlorites, by refining phase relations from high temperatures experiments. Several low temperature calorimetry measurements had been performed on clay minerals, like the works of Robie et al. (1976) or Bertoldi et al. (2005), in order to obtain the entropy of illite and berthierine, respectively. In addition, a lot of solution experiments had been performed since the work Reesman and Keller (1968). Given the selection guidelines reported previously, these data are not considered for this selection. The datasets are reported in Table 2. The first part of the table groups a list of consistent datasets from direct measurements collected in the literature. The second part encloses a list of datasets extracted from equilibrium experiments usually performed a rather high temperature and pressures. This is especially the case for Chlorites. The third part is devoted to data measured and published in the framework of the Thermochimie project.

±

Table 2 - Thermodynamic properties of phyllosilicates selected for the present document.

Mineral	Formula	$\Delta H_{f,exp}^{\circ}$ kJ.mol ⁻¹	Ref.	S°_{conf} J.mol ⁻¹ .K ⁻¹	$S^{\circ}_{Tot}(2)$ J.mol ⁻¹ .K ⁻¹	Ref.	V_{exp}° cm ³ .mol ⁻¹	Ref.	Cp (25°C) J.mol ⁻¹ .K ⁻¹	a J.mol ⁻¹ .K ⁻¹	b*10 ³ J.mol ⁻¹ .K ⁻²	c*10 ⁻⁵ J.mol ⁻¹ .K	Ref
Phyllosilicates : direct measurements from literature													
Muscovite	KAl ₃ Si ₃ O ₁₀ (OH) ₂	-5974.80±4.9	95has/cyg		287.70±0.6	76rob/hem	140.81	95rob/hem	325.99	335.80	232.25	-70.27	76rob/hem
Pyrophyllite	Al ₂ Si ₄ O ₁₀ (OH) ₂	-5640.00±1.5	95rob/hem		239.40±0.4	95rob/hem	128.10	95rob/hem	293.76	314.07	198.15	-70.57	76rob/hem
Kaolinite	Al ₂ Si ₂ O ₅ (OH) ₄	-4115.30±4.1	01fia/nav		200.90±0.5	91rob/hem	99.34	95rob/hem	243.37	277.18	130.42	-64.62	91rob/hem
Dickite	Al ₂ Si ₂ O ₅ (OH) ₄	-4099.80±4.8	03fia/maj		197.10±1.3	61kin/wel	98.56	95rob/hem	239.56	268.92	147.15	-65.10	61kin/wel
Halloysite	Al ₂ Si ₂ O ₅ (OH) ₄	-4092.60±5.6	99del/nav		203.30±1.3	61kin/wel	99.30	78rob/hem	246.30				61kin/wel
Phlogopite	KMg ₃ Si ₃ O ₁₀ (OH) ₂	-6215.00±3.5	92cir/nav		315.90±1.0	84rob/hem	149.65	95rob/hem	354.65	400.17	163.02	-84.60	84rob/hem
Annite	KFe ₃ Si ₃ O ₁₀ (OH) ₂	-5130.97±8.3	95dac/ben		424.02±8.4	95dac/ben	154.30	95rob/hem	390.32	432.30	187.44	-87.40	95rob/hem
Talc	Mg ₃ Si ₄ O ₁₀ (OH) ₂	-5892.10±4.0	01kah/mar		260.80±0.6	63rob/sto	136.20	95rob/hem	321.77	420.72	90.46	-112.98	79kru/rob
Paragonite	NaAl ₃ Si ₃ O ₁₀ (OH) ₂	-5937.50±3.0	96rou/hov		277.10±0.9	84rob/hem	132.10	95rob/hem	321.50	349.98	200.51	-79.09	84rob/hem
Lizardite	Mg ₃ Si ₂ O ₅ (OH) ₄	-4363.50±3.0	95rob/hem		216.30±0.8	04eva	107.50	95rob/hem	274.05	296.63	167.14	-64.29	95rob/hem
Margarite	CaAl ₂ Si ₂ O ₁₀ (OH) ₂	-6244.00±2.6	95rob/hem		263.60±0.3	95rob/hem	129.63	95rob/hem	323.41	373.08	171.60	-91.35	82rob/haa
Phyllosilicates properties from high temperature and pressure equilibrium													
Greenalite	Fe ₃ Si ₂ O ₅ (OH) ₄	-3301.00	83miy/kle		304.50	83miy/kle	115.00	83miy/kle	302.32	303.39	166.34	-45.04	83miy/kle
Minnesotaite	Fe ₃ Si ₄ O ₁₀ (OH) ₂	-4822.99	83miy/kle		350.80	83miy/kle	148.50	83miy/kle	364.40	411.38	125.52	-75.03	83miy/kle
CeladoniteMg	KMgAlSi ₄ O ₁₀ (OH) ₂	-5844.48	98hol/pow	11.53	290.00	98hol/pow	139.57	98hol/pow	325.75	357.08	205.51	-82.32	98hol/pow
CeladoniteFe	KFeAlSi ₄ O ₁₀ (OH) ₂	-5497.32	98hol/pow	11.53	317.47	98hol/pow	140.70	98hol/pow	331.48	354.09	215.67	-77.26	98hol/pow
Eastonite	KMg ₃ Al ₂ Si ₂ O ₁₀ (OH) ₂	-6348.94	98hol/pow	10.60	306.00	98hol/pow	147.51	98hol/pow	350.10	408.09	156.53	-93.04	98hol/pow
Siderophyllite	KMg ₃ Al ₂ Si ₂ O ₁₀ (OH) ₂	-5628.27	90hol/pow	10.60	375.00	90hol/pow	150.63	90hol/pow	363.14	393.17	190.84	-77.27	90hol/pow
Amesite	Mg ₄ Al ₂ (Al ₂ Si ₂ O ₁₀ (OH) ₈	-9035.90	05vid/par		403.20	05vid/par	205.20	05vid/par	540.47	600.70	340.86	-143.88	05vid/par
Fe-Amesite	Fe ₄ Al ₂ (Al ₂ Si ₂ O ₁₀ (OH) ₈	-7607.46	05vid/par		514.80	05vid/par	209.00	05vid/par	564.74	595.11	375.34	-126.48	05vid/par
Clinochlore	Mg ₅ Al(AISi ₃)O ₁₀ (OH) ₈	-8909.59	05vid/par		435.15	05vid/par	211.47	05vid/par	516.34	631.95	282.68	-177.69	05vid/par
Chamosite	Fe ₅ Al(AISi ₃)O ₁₀ (OH) ₈	-7120.85	05vid/par		559.40	05vid/par	215.88	05vid/par	574.76	599.55	372.80	-120.85	05vid/par
Sudoite	Mg ₂ Al ₄ Si ₃ O ₁₀ (OH) ₈	-8655.27	05vid/par		390.50	05vid/par	205.10	05vid/par	509.72	557.84	351.23	-135.86	05vid/par
Phyllosilicates, properties measured within the framework of Thermochimie													
Ripidolite Cca-2	(1)	-8240.14±8.6	14bla/gai		469.19±2.9	14bla/gai	211.83	14bla/gai	547.02	590.91	384.01	-140.60	14bla/gai
Berthierine	(8)	-3768.95±6.26	14bla/gai		257.00±6.7	14bla/gai	101.16	14bla/gai	263.37				14bla/gai
Smectite MX80	(2)	-5656.37±5.4	12gai/bla	24.41	301.92±0.2	12gai/bla	134.92	12gai/bla	322.74	319.57	282.08	-72.97	12gai/bla
Smectite MX80, 3.989H ₂ O	(2) + 3.989H ₂ O	-6823.33±7.5	12gai/bla	24.41	558.27±0.3	12gai/bla	207.00	(11)	626.94				12gai/bla
Smectite MX80, 5.189H ₂ O	(2) + 5.189H ₂ O	-7174.42±9.2	12gai/bla	24.41	621.58±0.4	12gai/bla	228.69	(11)	712.77	491.66	740.53	0.24	12gai/bla
Illite IMt-2	(3)	-5711.25±8.5	12gai/bla	29.86	324.92±0.2	12gai/bla	139.18	12gai/bla	328.21	317.44	279.13	-64.51	12gai/bla
Beidellite SBId-1	(6)	-5720.69±6.5	12gai/bla	21.43	293.52±0.4	12gai/bla	137.98	12gai/bla	318.58	270.93	342.91	-48.60	12gai/bla
Beidellite SBId-1, 4.756H ₂ O	(6) + 4.756H ₂ O	-7059.45±5.2	12gai/bla	21.43	574±28	12gai/bla	223.92	(12)					12gai/bla
Nontronite Nau-1	(4)	-5035.69±5.3	13gai/bla	24.87	332.75±7.0	13gai/bla	136.38	13gai/bla	335.17	289.85	363.09	-55.96	13gai/bla

Mineral	Formula	$\Delta H_{f,exp}^{\circ}$ kJ.mol ⁻¹	Ref.	S°_{conf} J.mol ⁻¹ .K ⁻¹	$S^{\circ}_{Tot}(2)$ J.mol ⁻¹ .K ⁻¹	Ref.	V_{exp}° cm ³ .mol ⁻¹	Ref.	Cp (25°C) J.mol ⁻¹ .K ⁻¹	a J.mol ⁻¹ .K ⁻¹	b*10 ³ J.mol ⁻¹ .K ⁻²	c*10 ⁻⁵ J.mol ⁻¹ .K	Ref
Illite/smectite ISCz-1	(7)	-5787.22±7.5	19gai/bla	28.89	295.36±6.0	19gai/bla	137.13	19gai/bla	306.00	236.14	422.80	-49.92	19gai/bla
Saponite SapCa1	(5)	-5994.06±4.9	13gai/bla	17.83	314.55±1.6	13gai/bla	141.66	13gai/bla	347.19	347.26	274.68	-73.05	13gai/bla
Vermiculite SO	(9)	-6034.41±5.7	13gai/bla	26.66	325.77±0.5	13gai/bla	148.36	13gai/bla	346.70	329.42	313.22	-67.82	13gai/bla
Other phases													
Antigorite	Mg ₄₈ Si ₃₄ O ₈₅ (OH) ₆₂	-71417.98	98hol/pow		3591.00	98hol/pow	1754.80	98hol/pow	4380.66	4952.60	2422.78	-1150.54	98hol/pow
Chrysotile	Mg ₃ Si ₂ O ₅ (OH) ₄	-4360.00±3.0	04eva/ 95rob/hem		221.30±0.8	95rob/hem	107.50	95rob/hem	274.05	296.63	167.14	-64.29	95rob/hem
Sepiolite	Mg ₄ Si ₆ O ₁₅ (OH) ₂ .6H ₂ O	-10109.55	88sto		670.00	88sto	285.50	88sto	736.41	778.00	268.00	-108.00	88sto
Lizardite MFN3	(10)	-4324.80±3.7	19gai/bla	12.24	226.08±4.9	19gai/bla	107.37	19gai/bla	275.76	221.42	337.47	-41.13	19gai/bla

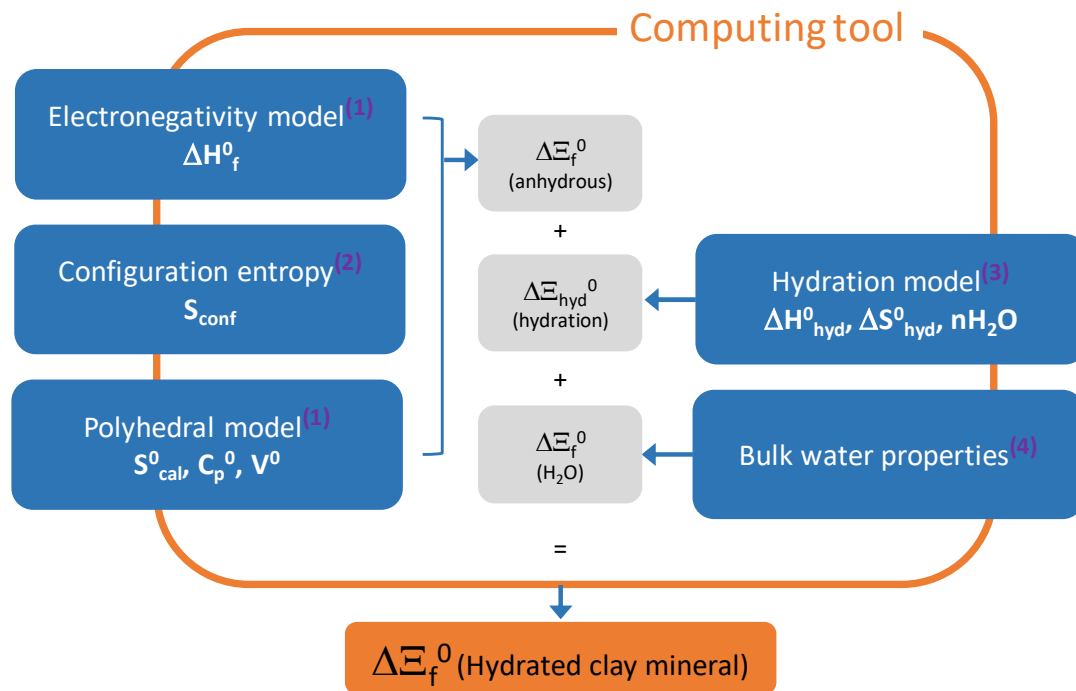
Formulas : (1) $(Mg_{2.964}Fe^{2+}_{1.712}Fe^{3+}_{0.215}Al_{1.116}Ca_{0.011})(Si_{2.633}Al_{1.367}O_{10}(OH)_8)$; (2) $Na_{0.409}K_{0.024}Ca_{0.009}(Si_{3.738}Al_{0.262})(Al_{1.598}Mg_{0.214}Fe^{3+}_{0.173}Fe^{2+}_{0.035}O_{10}(OH)_2)$;
(3) $K_{0.762}Na_{0.044}(Si_{3.387}Al_{0.613})(Al_{1.427}Fe^{3+}_{0.292}Mg_{0.241}Fe^{2+}_{0.084}O_{10}(OH)_2$; (4) $Ca_{0.247}K_{0.020}(Si_{3.458}Al_{0.542})(Fe^{3+}_{1.688}Al_{0.276}Mg_{0.068}O_{10}(OH)_2$;
(5) $(Na_{0.394}K_{0.021}Ca_{0.038})(Si_{3.569}Al_{0.397})(Mg_{2.949}Fe_{0.034}^{3+}Fe_{0.021}^{2+})O_{10}(OH)_2$; (6) $Ca_{0.185}K_{0.104}(Si_{3.574}Al_{0.426})(Al_{1.812}Mg_{0.090}Fe^{3+}_{0.112}O_{10}(OH)_2$
(7) $(Ca_{0.092}K_{0.439})(Si_{3.562}Al_{0.438})(Al_{1.732}Mg_{0.255}Fe^{3+}_{0.029}Fe^{2+}_{0.011})O_{10}(OH)_2$; (8) $(Si_{1.332}Al_{0.668})(Al_{0.976}Fe^{3+}_{0.182}Fe^{2+}_{1.44}Mg_{0.157}O_5(OH)_4$
(9) $Ca_{0.445}(Si_{2.778}Al_{1.222})(Al_{0.216}Mg_{2.475}Fe^{3+}_{0.226}Fe^{2+}_{0.028}O_{10}(OH)_2$
(10) $(Si_{1.917}Al_{0.065}Fe^{3+}_{0.018})(Mg_{2.736}Al_{0.115}Fe^{3+}_{0.048}Fe^{2+}_{0.094}O_{5.066}(OH)_{3.934}$
(11) After Gailhanou et al. (2012) for the anhydrous part and considering that $V_{H_2O} = 18.07$ cm³/mol
(12) After Blanc and Vieillard (2010) for the anhydrous part and considering that $V_{H_2O} = 18.07$ cm³/mol

6. Developments of models for thermodynamic properties prediction

The development of prediction models is splitted into 1) models for the properties of formation of the anhydrous clay minerals and 2) models for the hydration reaction when the mineral requires it.

6.1. GLOBAL SCHEME TO DEVELOP PREDICTIVE MODELS

Regarding clay minerals, in order to estimate the whole set of thermodynamic parameters, including the hydration properties, it is necessary to combine models able to predict anhydrous phase properties and models able to calculate the hydration properties. Such a methodology had been previously followed by Vidal and Dubacq (2009) and Dubacq et al. (2010), who combined their own hydration model with Chermak and Rimstidt's work (Chermak and Rimstidt, 1989), for the anhydrous part. Similarly, in this study, the estimation of thermodynamic properties for hydrated clay minerals is achieved by merging the model of Blanc et al. (2015) for the anhydrous part and the model developed by Gailhanou et al. (2017) and Vieillard et al. (2019) for hydration. The whole process is illustrated in Figure 4.



⁽¹⁾ Vieillard et al. (1994a and b), Blanc et al. (2015) ; ⁽²⁾ Ulrich and Waldbaum (1976) ; ⁽³⁾ Gailhanou et al. (2017), Vieillard et al. (2019) ; ⁽⁴⁾ Cox et al. (1989)

Figure 4 - General scheme indicating the relations between estimation models to provide thermodynamic properties for hydrated clay minerals.

6.2. PREDICTIVE MODELING OF THE THERMODYNAMIC PROPERTIES OF FORMATION OF ANHYDROUS CLAY MINERALS

6.2.1. Existing models

To determine the missing thermodynamic parameters of a clay phase whose chemical composition is known, different methods were developed using thermodynamic data of silicates to estimate the major thermodynamic parameters (V , ΔG_f^0 , ΔH_f^0 , S^0 , C_{pTr}).

Most of the predicting models are based on the assumption that the thermodynamic properties of a mineral can be obtained by combining the properties of its constituents. They may be simple elements (Latimer, 1951), oxides (Karpov and Kashik, 1968), or hydroxides (Sposito, 1986). This technique has been significantly improved by taking into account the coordination polyhedron of cations in mineral structures (polyhedral decomposition models: Hazen (1985), Hazen (1988), Chermak and Rimstidt (1989), Holland (1989b), Van Hinsberg et al. (2005a)). In any case, the basic principles remains, that is: 1) to collect a set of calibration phases; 2) to decompose those phases into the base units retained and 3) to calibrate the properties of each base unit by minimizing the sum of squared differences between observed and predicted values for the calibration set of minerals.

A different type of model is based on the approach developed by Vieillard, (1994a and b). The principle of calculation relies on the difference in electronegativity between two cations around a common oxygen atom. It is especially efficient in predicting formation enthalpy, the reason why it was retained.

6.2.2. Method of prediction for the enthalpy of formation based on the electronegativity difference

Fundamental developments

The methods is essentially based on the concept of the electronegativity χ , of Pauling (1960) which is the power of an atom in a molecule to attract electrons from another atom. Let us consider a binary oxide compound ABO_N , (where A and B are different cations), that may decompose in a sum of two oxides AO_{n1} and BO_{n2} , the energy of formation of ABO_N can be written as:

$$E(ABO_N) = E(AO_{n1}) + E(BO_{n2}) + kX_A X_B (\chi_A - \chi_B)^2 \quad \text{Eq. 20}$$

The third term, representing the energy of formation of the compound from AO_{n1} and BO_{n2} oxides, is proportional, in the first hand, to the molar fraction of oxygens atoms. The latter are respectively related to the cations A (X_A) and B (X_B) of the oxides AO_{n1} and BO_{n2} in the formation of binary compound, and, in the second hand, to the difference in electronegativity between the cations A and B on a common oxygen atom. Greater is the difference in electronegativity between the cations on oxygen, stronger will be the energy of formation of the compound. If two cations linked to the same atom of oxygen, have a same electronegativity or are identical, the energy of formation from the oxides is null. If two cations have different electronegativities and are not bound by a common oxygen atom, the energy of formation is zero or negligible.

Application: the ΔH_f^0 , 298 of anhydrous phyllosilicates

Thanks to recent measurements of the enthalpies of formation of the anhydrous phyllosilicates developed within the framework of Thermochimie project, Vieillard (2006) proposed to build a model for the prediction of the enthalpies of formation of the anhydrous phyllosilicates including the three structural families (7, 10 and 14Å). This model, based on the (Vieillard, 1994a)'s

algorithm, could be simplified by assuming that the parameter $\Delta_{\text{H}}\text{O}^{\text{M}^{2+}}(\text{clay})$, characterizing the electronegativity of the cation M^{2+} in a specific site is constant and independent of the interatomic variations of distances in the various sites. Full details are given in Blanc et al. (2015). The parameterization used 28 phyllosilicates, of which the thermodynamic properties are reported in Table 2, to determine a set of parameters $\Delta_{\text{H}}\text{O}^{\text{M}^{2+}}(\text{clay})$ for 16 cations distributed in the various structural sites of the phyllosilicates: Na^+ , K^+ , Ca^{2+} in the interlayer sites, Mg^{2+} , Fe^{2+} , Fe^{3+} , Al^{3+} in octahedral and in brucitic sites, Al^{3+} and Si^{4+} in tetrahedral sites, H^{o} , H^{b} and H^{e} in the different sites. The parameter $\Delta_{\text{H}}\text{O}^{\text{M}^{2+}}(\text{clay})$ characterizes the electronegativity of the cation i in the crystalline environment of the mineral.

In Figure 5 are represented the results obtained for both the parameterization and the verification datasets. Calculations are compared with results obtained using Chermak and Rimstidt (1989) method. For only one mineral, vermiculite, the enthalpy of formation predicted by using the electronegativity model is lower than -0.5% from the measured value. Globally, estimates by the Chermak and Rimstidt (1989) method display a wider range of discrepancies and a more important systematic deviation than the calculation performed by using the model developed here.

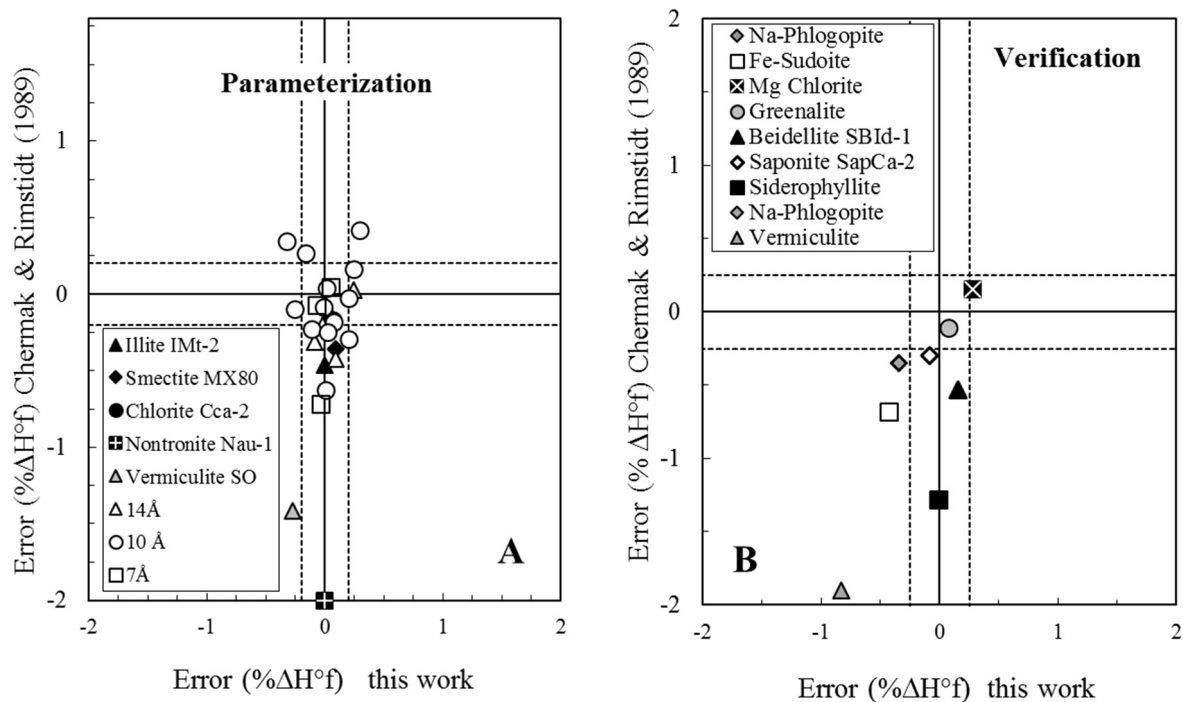


Figure 5 - Enthalpy of formation of phyllosilicates: comparison of the discrepancy of the estimates, calculated either with the present model or with the method of Chermak and Rimstidt (1989). A- Parameterization phases; B- Verification phases.

6.2.3. Polyhedral method for entropy and heat capacity

The principle is to describe the thermodynamic functions as a linear combination of the mineral stoichiometric composition, including, in some cases, additional physical variables, such as volume for instance (Holland, 1989). The mineral structural formulas are decomposed into a

sum of oxides and/or hydroxides of all cations, in such a way that the properties (ΔG_r^0 , ΔH_r^0 , ΔS_r^0 , ΔV_r , $\Delta C_{p,r}$) of fictive solid-solid reactions are zero.

Mathematical formalism

Considering a set of four phases (a, b, c and d) and the property X, and assuming that each of the four phases can be decomposed into three elementary polyhedrons (pol₁, pol₂ and pol₃), the polyhedral decomposition consists in calculating the coordinates of each phase with respect to the three X_{pol} polyhedrons. In equation (21), the result of this calculation corresponds to the "Coordinates" matrix, which relates the matrix of the X mineral values, X_{min}, to the matrix of X for each polyhedron, X_{pol}:

$$\begin{pmatrix} X_{\min}^a \\ X_{\min}^b \\ X_{\min}^c \\ X_{\min}^d \end{pmatrix} = \begin{pmatrix} c_1^a & c_2^a & c_3^a \\ c_1^b & c_2^b & c_3^b \\ c_1^c & c_2^c & c_3^c \\ c_1^d & c_2^d & c_3^d \end{pmatrix} \cdot \begin{pmatrix} X_{\text{pol}1} \\ X_{\text{pol}2} \\ X_{\text{pol}3} \end{pmatrix} \quad \text{Eq. 21}$$

This relation implies that the number of mineral phases (a, b, c, d) is higher or equal to the number of polyhedrons (pol₁, pol₂, pol₃). The X_{pol} values are obtained by minimizing the squared difference between X_{min(obs)} and X_{min(calc)}, which corresponds to the SSD (Sum of Squared Differences) parameter in the following equation:

$$\text{SSD} = \sum_{i=1}^n (X_{\min}^i(\text{obs}) - X_{\min}^i(\text{calc}))^2 \quad \text{with} \quad X_{\min}^i(\text{calc}) = \sum_{j=1}^m X_{\text{pol}j} \cdot c_j^i \quad \text{Eq. 22}$$

The model is applied to the properties lattice entropy S^{lat}, volume V, and for the heat capacity C_p(T) function, to each of the Mayer-Kelley coefficients a, b and c.

Verification of the polyhedral model

As for the enthalpy of formation, the verification is carried out using an independent dataset, apart from the set used for model parameterization. For the entropy estimate, Figure 6 compares the discrepancy with values estimated using either the present method or that of Holland (1989). For Holland (1989), we have considered it *a priori* the most effective method, including a contribution that depends on the molar volume. The method proposed here exhibits results that fall within the ± 5% domain, except for one point at -8.5%, which corresponds to the Mg-chlorite. For the Holland (1989) method (Fig. 3), the discrepancies are larger, between +3 and -13%, and exhibit a clear systematic overestimation close to 5%, which has already been reported by Gailhanou et al. (2013).

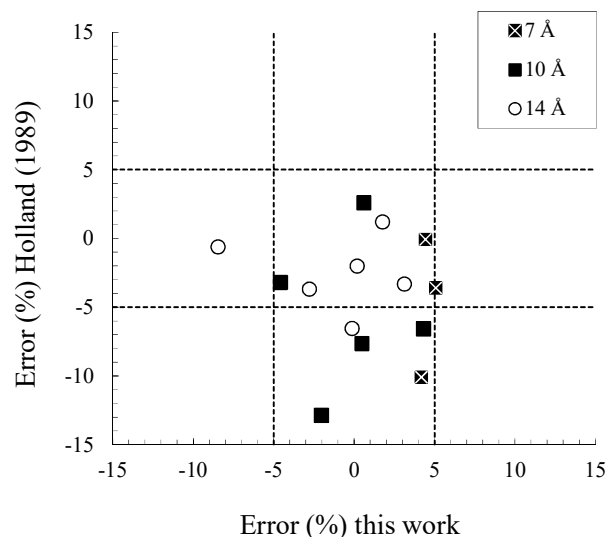


Figure 6 - Verification of the predicted entropy: comparison between two different estimating method methods. $Error (\%) = (S^{lat}_{obs} - S^{lat}_{calc}) / S^{lat}_{obs} * 100$; S^{lat}_{obs} values and references as reported in Table 2 for the different minerals.

6.2.4. Predicting the Gibbs energy of anhydrous phases

By combining the estimates of the enthalpy of formation and the entropy through equation (1), it is possible to predict the Gibbs free energy values. Since the accuracy of predictions for ΔH^0_f and S^{lat} have already been checked, the main question arises from the additional entropy terms from equation (3), S^{mag} and S^{conf} . For chamosite for example, S^{mag} reaches 66.91 J/mol.K. This contributes up to -20 kJ/mol to the final value of ΔG^0_f and modifies it by -0.28%. Such modification is far from negligible and it needs to be tested. Calculations were performed in Blancet al. (2015), and the results are compared to the experimentally measured ΔG^0_f values in Figure 7. For the verification minerals, Figure 7.B indicates that the combination of the different entropy terms tends to reduce the overall uncertainty for ΔG^0_f estimates.

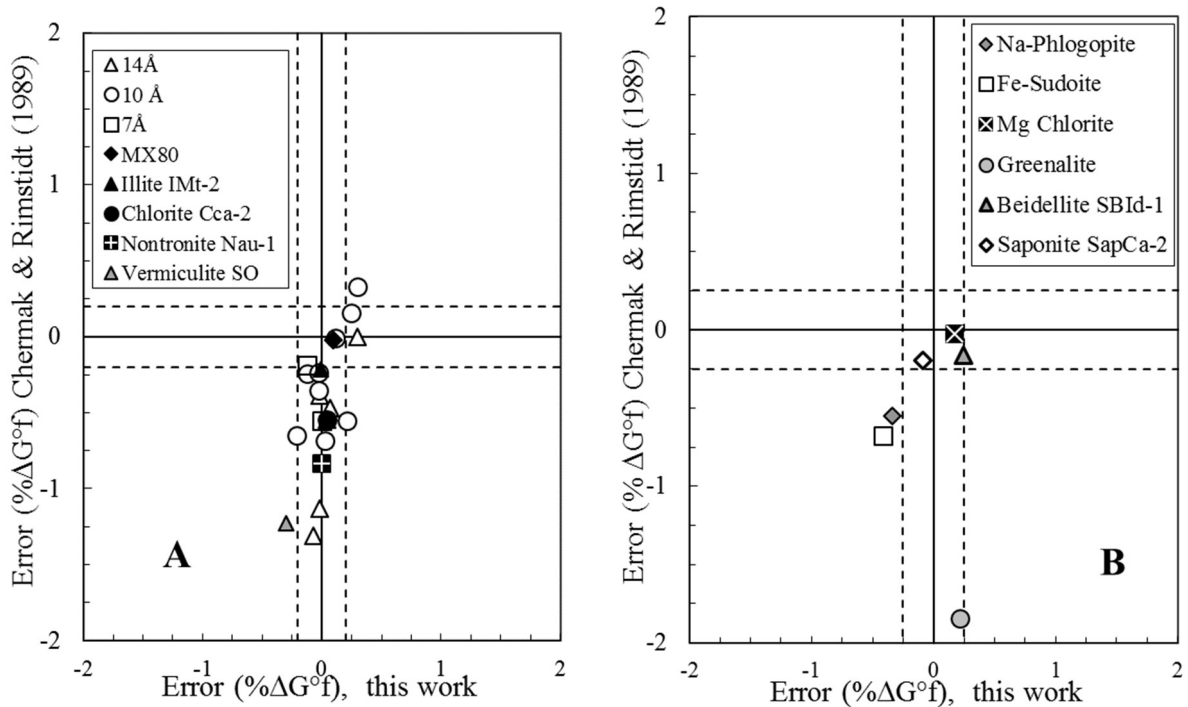


Figure 7 - Predicted ΔG_f^0 for phyllosilicates: comparison of the discrepancy between experimental measurements and values calculated either with the present model or with the method of Chermak and Rimstidt (1989). A) Phases for parameterization; B) Verification phases.

6.3. PREDICTIVE MODELING OF THE THERMODYNAMIC PROPERTIES OF THE HYDRATION OF CLAY MINERALS

To predict the properties of hydration, the method described by Gailhanou et al. (2017) uses a stage intermediate between the raw data extracted from adsorption isotherm and hydration predicted energies. It consist in parameterize a binary solid solution model to estimate the amount and the thermodynamic properties of clay water depending on pressure, temperature and relative humidity. The prediction calculation are realized thereafter, extending the solid solution model to clay water in other 2:1 clay compositions by:

- (i) establishing chemical relationships between the parameters of the solid solution models and the chemical composition of the 2:1 clays;
- (ii) generalizing the solid solution model for 2:1 clays;
- (iii) assessing the model based on the comparison with experimental data provided by literature.

The overall approach is depicted in Figure 8.

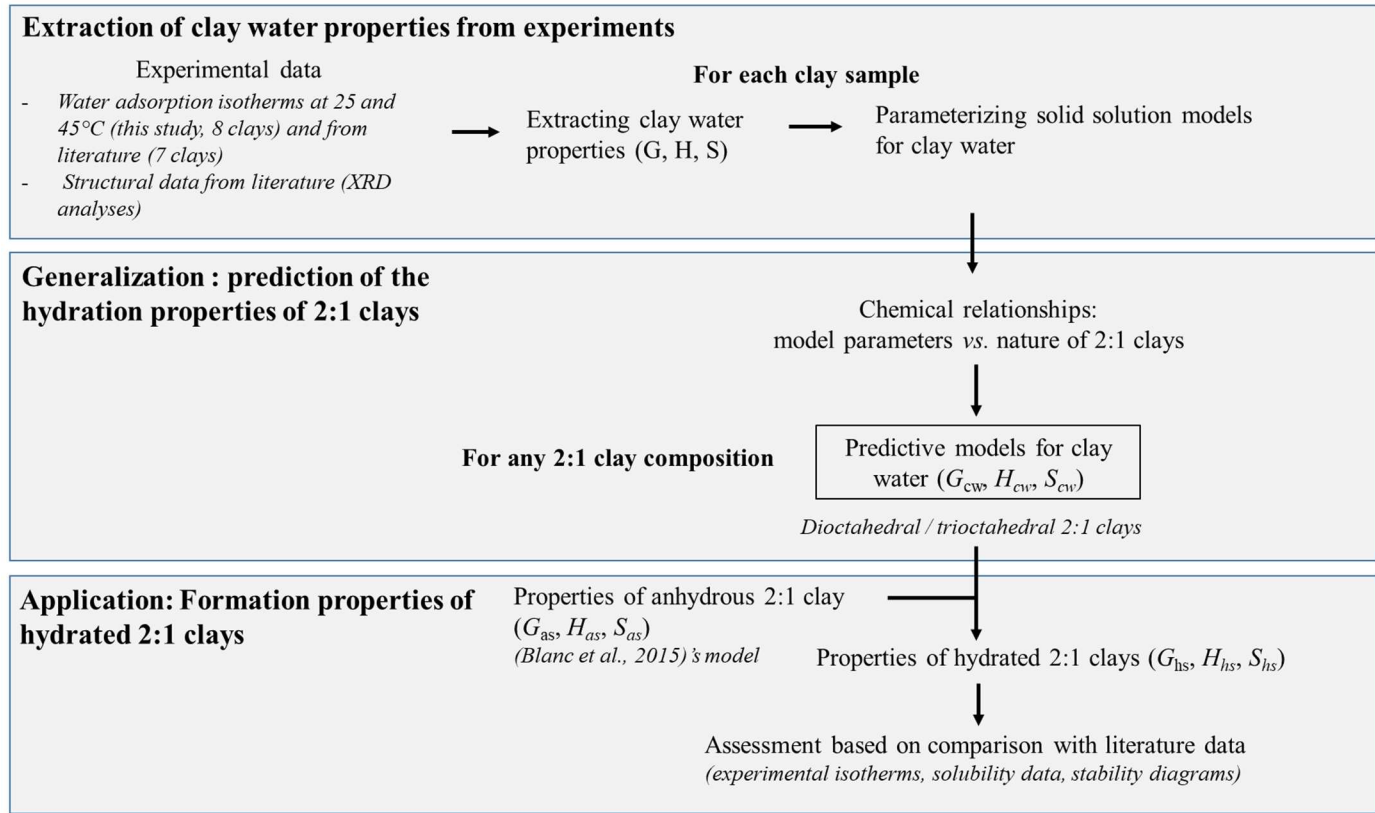


Figure 8 - Schematic representation of the overall approach developed for the generalization of the solid solution models to smectites.

The theoretical relations used in the process illustrated by Figure 8 are fully detailed in Gailhanou et al. (2017) and Vieillard et al. (2019). In short, these authors are considering the equilibrium constant for the hydration reaction as:

$$\log_{10}K = -\frac{\Delta_{\text{Cem.W}}G_{T,P}}{R \cdot T \cdot \ln(10)} \quad \text{Eq. 23}$$

where $\Delta_{\text{Cem.W}}G_{T,P} = \Delta G_{f,\text{Cem.W}}^0 - \Delta G_{f,\text{Cem}}^0 - n_{\text{Cem.W}}\Delta G_{f,W}^0$ is the Gibbs free energy of hydration per mole of clay, at any temperature T and pressure P, from the anhydrous state to the maximum hydration state. It represents the theoretical energy necessary to form the hydrated end-member from the anhydrous end-member. It is related to the enthalpy of hydration ($\Delta_{\text{Cem.W}}H_{T,P}$) and the entropy of hydration ($\Delta_{\text{Cem.W}}S_{T,P}$) by the relation:

$$\Delta_{\text{Cem.W}}G_{T,P} = \Delta_{\text{Cem.W}}H_{T,P} - T \cdot \Delta_{\text{Cem.W}}S_{T,P} \quad \text{Eq. 24}$$

Vieillard et al. (2011) have decomposed the non-ideal W_G interaction into an enthalpic (W_H) and an entropic (W_S) term. In that case, the integral enthalpy and the integral entropy of hydration are given by:

$$\Delta_{\text{Cem.W}}H_{T,P} = \frac{1}{n_{\text{Cem.W}}} \int_0^x x_{\text{Cem.W}} \cdot \Delta_{\text{Cem.W}}\bar{h}_{T,P} + x_{\text{Cem.W}} \cdot (1-x_{\text{Cem.W}}) \cdot W_H \quad \text{Eq. 25}$$

and

$$\Delta_{\text{Cem.W}}S_{T,P} = \frac{1}{n_{\text{Cem.W}}} \int_0^x x_{\text{Cem.W}} \cdot \Delta_{\text{Cem.W}}\bar{s}_{T,P} - R[x_{\text{Cem.W}} \cdot \ln(x_{\text{Cem.W}}) + (1-x_{\text{Cem.W}}) \cdot \ln(1-x_{\text{Cem.W}})] + x_{\text{Cem.W}} \cdot (1-x_{\text{Cem.W}}) \cdot W_S \quad \text{Eq. 26}$$

with $W_G = W_H - T \cdot W_S$ and where $\Delta_{\text{Cem.W}}\bar{h}_{T,P}$ and $\Delta_{\text{Cem.W}}\bar{s}_{T,P}$ represent the differential enthalpy and entropy of hydration, respectively. The formation properties of clay water: $\Delta G_f(\text{H}_2\text{O})_{\text{Cem.W,T,P}}$, $\Delta H_f(\text{H}_2\text{O})_{\text{Cem.W,T,P}}$ and $S(\text{H}_2\text{O})_{\text{Cem.W,T,P}}$, are then obtained:

$$\Delta \Xi_f(\text{H}_2\text{O})_{\text{Cem.W}} = \Delta \Xi_f^0(\text{H}_2\text{O})_W + \Delta_{\text{Cem.W}}\Xi/n_{\text{Cem.W}} \quad \text{Eq. 27}$$

where $\Delta \Xi_f^0(\text{H}_2\text{O})_W$ designs the thermodynamic properties of liquid water in standard state and $\Delta_{\text{Cem.W}}\Xi$ represents the thermodynamic properties (G, H or S) of the hydration reaction of the clay from its anhydrous state to its full hydrated state, excluding capillary water. Eventually, four parameters $\Delta H_f(\text{H}_2\text{O})_{\text{Cem.W,T,P}}$ (or $\Delta_{\text{Cem.W}}H$), $S(\text{H}_2\text{O})_{\text{Cem.W,T,P}}$ (or $\Delta_{\text{Cem.W}}S$), W_H and W_S are required to fully describe the clay water/smectite equilibrium as a function of relative humidity, temperature and pressure.

To predict the four thermodynamic entities $\Delta_{\text{Cem. } W_H}$, $\Delta_{\text{Cem. } W_S}$, W_H and W_S characterizing the solid solution for clay water, four equations involving the interlayer charge (I.C.), the tetrahedral charge (T.C.) and the nature of the interlayer cation M^{z+} defined by $\Delta_{\text{H}O^=M^{z+}}$ for enthalpy and $S_{\text{hyd.}M^{z+}}$ for entropy may be written:

$$\Delta_{\text{Cem. } W_H}/\text{I.C.}/(1-\text{I.C.}) = a_H^*(\Delta_{\text{H}O^=M^{z+}})^*(\text{T.C.}) + b_H^*(\Delta_{\text{H}O^=M^{z+}}) + c_H^*(\text{T.C.}) + d_H \quad \text{Eq. 28}$$

$$W_H/\text{I.C.}/(1-\text{I.C.}) = a_{WH}^*(\Delta_{\text{H}O^=M^{z+}})^*(\text{T.C.}) + b_{WH}^*(\Delta_{\text{H}O^=M^{z+}}) + c_{WH}^*(\text{T.C.}) + d_{WH} \quad \text{Eq. 29}$$

$$\Delta_{\text{Cem. } W_S}/\text{I.C.}/(1-\text{I.C.}) = a_S^*(S_{\text{hyd.}M^{z+}})^*(\text{T.C.}) + b_S^*(S_{\text{hyd.}M^{z+}}) + c_S^*(\text{T.C.}) + d_S \quad \text{Eq. 30}$$

$$W_S/\text{I.C.}/(1-\text{I.C.}) = a_{WS}^*(S_{\text{hyd.}M^{z+}})^*(\text{T.C.}) + b_{WS}^*(S_{\text{hyd.}M^{z+}}) + c_{WS}^*(\text{T.C.}) + d_{WS} \quad \text{Eq. 31}$$

where a, b, c and d terms corresponds to empirical coefficients for the polynomial function.

These equations suppose linear relationships between the thermodynamic entities of hydration and both the nature of the clay mineral (characterized by its interlayer and tetrahedral charge) and the nature of the interlayer cation (characterized by its thermochemical properties $\Delta_{\text{G}O^=M^{z+}}$, $\Delta_{\text{H}O^=M^{z+}}$ and $S_{\text{hyd.}M^{z+}}$). The constant terms a, b, c and d can be determined by minimization of the difference between the calculated values from Eq. (28) to (31) and those obtained from the solid solution model. Two sets of equations are written in order to distinguish di-octahedral and tri-octahedral clays.

The results of prediction calculations are illustrated by Figures 9 and 10, for di-octahedral and tri-octahedral clays, respectively. In these figures, the location of the curve representing the solid solution model is systematically very close to the predictive calculation results, which allows assessing the accuracy of the predictive model.

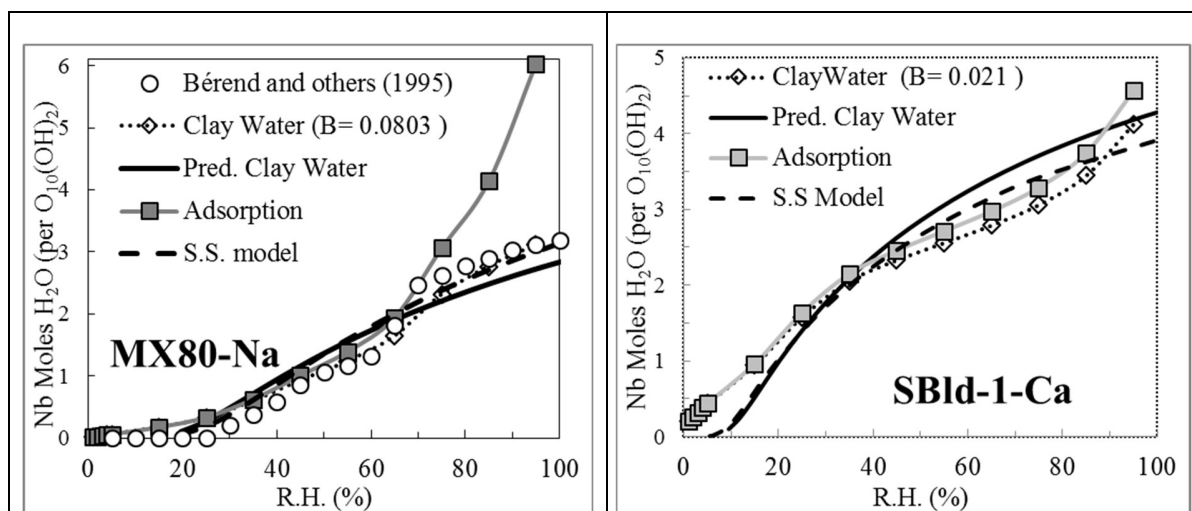


Figure 9 - Water adsorption isotherms at 298 K for different types of water in MX80-Na and SBld-1-Ca smectites (long dotted squares: total adsorbed water; circles: clay water isotherm from Berend et al. (1995); long dotted diamonds: clay water extracted from the experimental method; black line: dotted clay water estimated from the solid solution model; black line: clay water estimated from the predictive solid solution model).

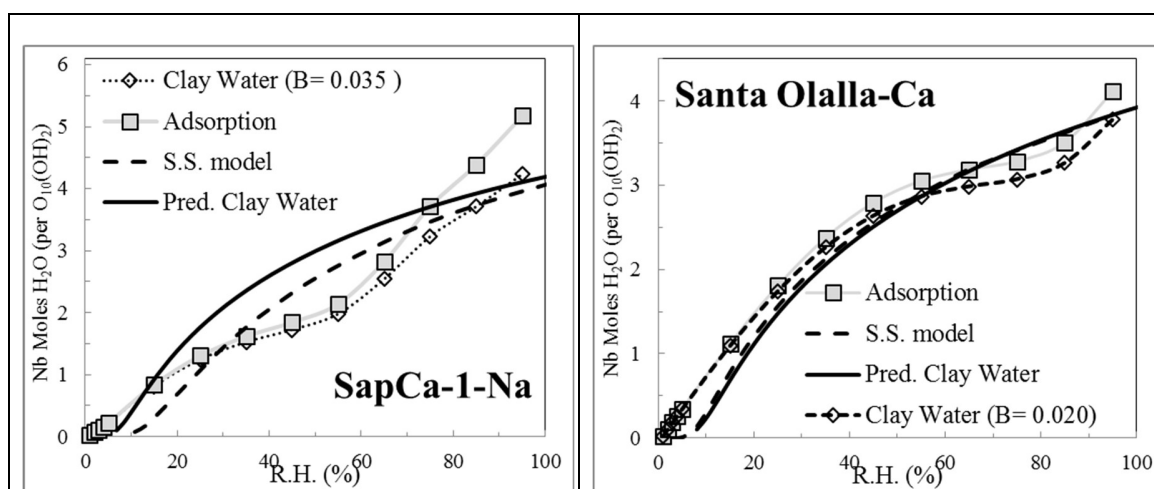


Figure 10 - Water adsorption isotherms at 298 K for different types of water in saponite SapCa-1-Na and Santa Olalla vermiculite-Ca (long dotted squares: total adsorbed water; long dotted diamonds: clay water extracted from the experimental method; dotted black line: clay water estimated from the solid solution model; black line: clay water estimated from the predictive solid solution model).

6.4. THERMODYNAMIC PROPERTIES ESTIMATED FOR THEORETICAL END MEMBERS

Modeling cement-clay interactions in the context of radioactive waste deep disposal implies to take advantage of a large database of clay minerals end-members in order to leave the reactions pathways as free as possible. In order to provide such a large database, we have used the predictive models detailed before.

The compositions of the clay end-members has been chosen in order to cover a large domain, including illite and smectite (di- and trioctahedral), Al/Fe/Mg substitutions in the octahedral sheet and 4 interlayer compositions (Na, K, Ca and Mg). For chlorites, the present models have been developed consistently with Vidal et al. (2005) work. The latter already proposed end-member compositions that make it possible to take into account a large composition domain and the present work relies on the thermodynamic properties refined by Vidal et al. (2005) for such phases. For the 7Å phases, we have estimated the properties of a cronstedtite and a berthierine. These stand for the extreme transformation products of a smectite in contact with iron, as determined by Mosser-Ruck et al. (2010).

The formation enthalpies, entropies, the $C_p(T)$ functions and volumes are calculated individually for different compositions of clay minerals. Then formation enthalpies and entropies are combined in order to provide the Gibbs free energy. The resulting properties set is reported in Table 3, where estimated entropies are including a configurational term, calculated according to the method of Ulbrich and Waldbaum (1976) (Ulbrich and Waldbaum (1976)).

In addition, the present document reports the thermodynamic properties of the hydrated clay mineral end members (Table 4). These are calculated using the predicting method from Gailhanou et al. (2017) and Vieillard et al. (2019) and shortly described previously. Calculations for the number of H₂O moles, the enthalpies and entropies of hydration are carried out at $P/P_0 = 1$ (water saturation).

Calculations were achieved using the tool developed by Blanc et al. (2021), where the models developed by Blanc et al. (2015) and Vieillard et al. (2019) are implemented. 2 differences arises for the 7Å minerals Berthierine(Fell) and Cronstedtite (Blanc et al. 2015, Table 14). Berthierine(Fell) $\Delta_f H^0$ displays a typographical error in Blanc et al. (2015) with -3770.46 instead of -3775.46 kJ.mol⁻¹. For Cronstedtite, the calculation from Blanc et al. (2015) was limited by using a ⁴¹Fe₂O₃ component assessed using Goethite properties. This component is fully integrated in the calculation tool which modifies the thermodynamic properties:

- Blanc et al. (2015): $\Delta_f H^0 = -2914.55$ kJ.mol⁻¹; $S^{\text{lat}} = 256.60$ J.mol⁻¹.K⁻¹; $C_p^0 = 257.02$ J.mol⁻¹.K⁻¹; $V^0 = 76.80$ cm³.mol⁻¹
- Blanc et al. (2021): $\Delta_f H^0 = -2916.68$ kJ.mol⁻¹; $S^{\text{lat}} = 289.91$ J.mol⁻¹.K⁻¹; $C_p^0 = 307.69$ J.mol⁻¹.K⁻¹; $V^0 = 90.44$ cm³.mol⁻¹.

Table 3 - Estimated thermodynamic properties of anhydrous clay minerals end members.

Mineral		Formula	ΔH_f^0 kJ.mol ⁻¹	S^{lat} J.mol ⁻¹ .K ⁻¹	$S^{conf.+S^{mag}}$ J.mol ⁻¹ .K ⁻¹	C_p (25°C) J.mol ⁻¹ .K ⁻¹	V° cm ³ .mol ⁻¹
Montmorillonite	(MgK)	$K_{0.34}Mg_{0.34}Al_{1.66}Si_4O_{10}(OH)_2$	-5703.51	260.13	12.91	311.33	134.69
Low-charge	(MgNa)	$Na_{0.34}Mg_{0.34}Al_{1.66}Si_4O_{10}(OH)_2$	-5690.41	264.97	12.91	310.60	133.96
	(MgCa)	$Ca_{0.17}Mg_{0.34}Al_{1.66}Si_4O_{10}(OH)_2$	-5690.29	255.94	11.37	305.88	135.58
	(MgMg)	$Mg_{0.17}Mg_{0.34}Al_{1.66}Si_4O_{10}(OH)_2$	-5676.01	256.61	11.37	304.71	131.58
Montmorillonite	(HcK)	$K_{0.6}Mg_{0.6}Al_{1.4}Si_4O_{10}(OH)_2$	-5757.74	280.59	15.75	319.96	138.75
High-charge	(HcNa)	$Na_{0.6}Mg_{0.6}Al_{1.4}Si_4O_{10}(OH)_2$	-5734.63	289.13	15.75	318.67	137.47
	(HcCa)	$Ca_{0.3}Mg_{0.6}Al_{1.4}Si_4O_{10}(OH)_2$	-5734.42	273.21	15.24	310.34	140.32
	(HcMg)	$Mg_{0.3}Mg_{0.6}Al_{1.4}Si_4O_{10}(OH)_2$	-5709.22	274.38	15.24	308.29	133.27
Saponite	(K)	$K_{0.34}Mg_3Al_{0.34}Si_{3.66}O_{10}(OH)_2$	-6010.39	280.25	13.71	334.54	141.69
	(Na)	$Na_{0.34}Mg_3Al_{0.34}Si_{3.66}O_{10}(OH)_2$	-5997.76	285.09	13.71	333.81	140.96
	(Ca)	$Ca_{0.17}Mg_3Al_{0.34}Si_{3.66}O_{10}(OH)_2$	-5998.44	276.07	12.17	329.09	142.57
	(Mg)	$Mg_{0.17}Mg_3Al_{0.34}Si_{3.66}O_{10}(OH)_2$	-5984.34	276.73	12.17	327.93	138.58
Saponite- Fe	(FeK)	$K_{0.34}Mg_2Fe^{+2}Al_{0.34}Si_{3.66}O_{10}(OH)_2$	-5645.53	299.08	42.96	344.95	144.27
	(FeNa)	$Na_{0.34}Mg_2Fe^{+2}Al_{0.34}Si_{3.66}O_{10}(OH)_2$	-5632.90	303.91	42.96	344.23	143.54
	(FeCa)	$Ca_{0.17}Mg_2Fe^{+2}Al_{0.34}Si_{3.66}O_{10}(OH)_2$	-5633.58	294.89	41.43	339.50	145.15
	(FeMg)	$Mg_{0.17}Mg_2Fe^{+2}Al_{0.34}Si_{3.66}O_{10}(OH)_2$	-5619.48	295.56	41.43	338.33	141.16
Nontronite	(K)	$K_{0.34}Fe^{+3}_{1.67}Al_{0.67}Si_{3.66}O_{10}(OH)_2$	-4994.27	277.64	46.04	334.23	132.85
	(Na)	$Na_{0.34}Fe^{+3}_{1.67}Al_{0.67}Si_{3.66}O_{10}(OH)_2$	-4981.64	282.47	46.04	333.50	132.12
	(Ca)	$Ca_{0.17}Fe^{+3}_{1.67}Al_{0.67}Si_{3.66}O_{10}(OH)_2$	-4982.32	273.45	44.50	328.78	133.74
	(Mg)	$Mg_{0.17}Fe^{+3}_{1.67}Al_{0.67}Si_{3.66}O_{10}(OH)_2$	-4968.22	274.12	44.50	327.62	129.74
Beidellite	(K)	$K_{0.34}Al_{2.34}Si_{3.66}O_{10}(OH)_2$	-5749.86	252.94	13.71	310.35	133.22
	(Na)	$Na_{0.34}Al_{2.34}Si_{3.66}O_{10}(OH)_2$	-5737.23	257.78	13.71	309.62	132.49
	(Ca)	$Ca_{0.17}Al_{2.34}Si_{3.66}O_{10}(OH)_2$	-5737.91	248.76	12.17	304.90	134.10

Mineral	Formula	ΔH_f^0 kJ.mol ⁻¹	S^{lat} J.mol ⁻¹ .K ⁻¹	$S^{conf.}+S^{mag}$ J.mol ⁻¹ .K ⁻¹	C_p (25°C) J.mol ⁻¹ .K ⁻¹	V° cm ³ .mol ⁻¹
	(Mg) $Mg_{0.17}Al_{2.34}Si_{3.66}O_{10}(OH)_2$	-5723.81	249.42	12.17	303.74	130.11
Illite	(Mg) $K_{0.85}Mg_{0.25}Al_{2.35}Si_{3.4}O_{10}(OH)_2$	-5881.39	287.62	18.66	326.41	140.06
	(FeII) $K_{0.85}Fe^{+2}_{0.25}Al_{2.35}Si_{3.4}O_{10}(OH)_2$	-5796.29	292.22	22.01	329.00	140.67
	(FeIII) $K_{0.85}Fe^{+3}_{0.25}Al_{2.6}Si_{3.15}O_{10}(OH)_2$	-5795.39	286.03	22.08	329.28	138.92
	(Al) $K_{0.85}Al_{2.85}Si_{3.15}O_{10}(OH)_2$	-5913.65	282.33	12.08	325.70	138.98
Vermiculite	(K) $K_{0.86}Mg_3Si_{3.14}Al_{0.86}O_{10}(OH)_2$	-6173.41	310.21	12.15	350.19	147.56
	(Na) $Na_{0.86}Mg_3Si_{3.14}Al_{0.86}O_{10}(OH)_2$	-6143.26	322.45	12.15	348.34	145.71
	(Ca) $Ca_{0.43}Mg_3Si_{3.14}Al_{0.86}O_{10}(OH)_2$	-6148.06	299.63	14.47	336.40	149.80
	(Mg) $Mg_{0.43}Mg_3Si_{3.14}Al_{0.86}O_{10}(OH)_2$	-6113.11	301.31	14.47	333.46	139.69
Berthierine(FeIII)	$(Fe^{+2}_{2.34}Fe^{+3}_{0.33}Al_{0.33})(Si_{1.34}Al_{0.66})O_5(OH)_4$	-3457.44	251.74	36.23 ^(a)	297.41	103.27
Berthierine(FeII)	$(Fe^{+2}_2Al)(SiAl)O_5(OH)_4$	-3775.40	226.31	26.76 ^(a)	283.50	103.86
Cronstedtite	$(Fe^{+2}_2Fe^{+3})(SiFe^{+3})O_5(OH)_4$	-2916.68	289.91	56.56 ^(a)	257.02	76.80
Glauconite	$K_{0.75}(Mg_{0.25}Fe^{+2}_{0.25}Fe^{+3}_{1.25}Al_{0.25})$ $(Al_{0.25}Si_{3.75})O_{10}(OH)_2$	-5151.14	314.92	51.66	344.54	139.76

(a) Phase Si, Al ordered and configurational entropy is not considered, following Bertoldi et al. (2007).

Table 4 - Predicted values for the thermodynamic properties of hydration and of formation for theoretical hydrated clay mineral end-members (R.H. 100%).

Mineral		Formula	n_{CW}^*	$\Delta_{Cem.WH}$ kJ mol ⁻¹	$\Delta_{Cem.WS}$ J.mol ⁻¹ .K ⁻¹	ΔH_f^0 kJ.mol ⁻¹	S° J.mol ⁻¹ .K ⁻¹	C_p (25°C) J.mol ⁻¹ .K ⁻¹	V° cm ³ .mol ⁻¹
Montmorillonite	(MgK)	$K_{0.34}Mg_{0.34}Al_{1.66}Si_4O_{10}(OH)_2$	2.52	-10.64	-21.04	-6433.59	428.06	500.43	180.18
Low-charge	(MgNa)	$Na_{0.34}Mg_{0.34}Al_{1.66}Si_4O_{10}(OH)_2$	3.00	-16.43	-31.68	-6565.19	456.26	536.21	188.23
	(MgCa)	$Ca_{0.17}Mg_{0.34}Al_{1.66}Si_4O_{10}(OH)_2$	4.27	-31.23	-57.92	-6940.59	507.73	626.30	212.65
	(MgMg)	$Mg_{0.17}Mg_{0.34}Al_{1.66}Si_4O_{10}(OH)_2$	5.09	-38.27	-69.73	-7170.02	554.50	687.35	223.61
	(HcK)	$K_{0.6}Mg_{0.6}Al_{1.4}Si_4O_{10}(OH)_2$	2.51	-11.36	-22.82	-6487.39	449.31	508.77	184.16
High-charge	(HcNa)	$Na_{0.6}Mg_{0.6}Al_{1.4}Si_4O_{10}(OH)_2$	3.01	-17.60	-34.37	-6611.43	480.78	544.52	191.79
	(HcCa)	$Ca_{0.3}Mg_{0.6}Al_{1.4}Si_4O_{10}(OH)_2$	4.29	-33.58	-62.84	-6993.64	525.55	632.50	217.80
	(HcMg)	$Mg_{0.3}Mg_{0.6}Al_{1.4}Si_4O_{10}(OH)_2$	5.13	-41.19	-75.58	-7216.43	572.81	693.63	225.95
	(K)	$K_{0.34}Mg_3Al_{0.34}Si_{3.66}O_{10}(OH)_2$	4.06	-10.02	-5.11	-7181.17	572.91	639.65	215.07
Saponite	(Na)	$Na_{0.34}Mg_3Al_{0.34}Si_{3.66}O_{10}(OH)_2$	4.30	-13.61	-7.31	-7239.58	592.06	656.64	218.61
	(Ca)	$Ca_{0.17}Mg_3Al_{0.34}Si_{3.66}O_{10}(OH)_2$	4.80	-20.99	-13.14	-7391.13	610.78	689.64	229.29
	(Mg)	$Mg_{0.17}Mg_3Al_{0.34}Si_{3.66}O_{10}(OH)_2$	5.04	-22.86	-15.27	-7447.50	626.11	706.51	229.63
	(FeK)	$K_{0.34}Mg_2Fe^{+2}Al_{0.34}Si_{3.66}O_{10}(OH)$	4.06	-10.02	-5.11	-6816.30	621.00	650.05	217.65
Saponite- Fe	(FeNa)	$Na_{0.34}Mg_2Fe^{+2}Al_{0.34}Si_{3.66}O_{10}(OH)$	4.30	-13.61	-7.31	-6874.71	640.14	667.05	221.19
	(FeCa)	$Ca_{0.17}Mg_2Fe^{+2}Al_{0.34}Si_{3.66}O_{10}(OH)$	4.80	-20.99	-13.14	-7026.26	658.86	700.05	231.87
	(FeMg)	$Mg_{0.17}Mg_2Fe^{+2}Al_{0.34}Si_{3.66}O_{10}(O)$	5.04	-22.86	-15.27	-7082.64	674.19	716.91	232.21
	(K)	$K_{0.34}Fe^{+3}_{1.67}Al_{0.67}Si_{3.66}O_{10}(OH)_2$	1.63	-7.54	-19.56	-5466.86	417.93	456.47	162.25
Nontronite	(Na)	$Na_{0.34}Fe^{+3}_{1.67}Al_{0.67}Si_{3.66}O_{10}(OH)$	2.76	-12.08	-26.84	-5781.46	494.46	540.56	181.92
	(Ca)	$Ca_{0.17}Fe^{+3}_{1.67}Al_{0.67}Si_{3.66}O_{10}(OH)$	4.24	-22.80	-39.39	-6217.04	575.14	647.33	210.35
	(Mg)	$Mg_{0.17}Fe^{+3}_{1.67}Al_{0.67}Si_{3.66}O_{10}(OH)$	4.10	-25.74	-45.66	-6165.29	559.61	635.50	203.79
	(K)	$K_{0.34}Al_{2.34}Si_{3.66}O_{10}(OH)_2$	1.63	-7.54	-19.56	-6222.45	360.91	432.59	162.62
Beidellite	(Na)	$Na_{0.34}Al_{2.34}Si_{3.66}O_{10}(OH)_2$	2.76	-12.07	-26.83	-6537.05	437.44	516.68	182.29
	(Ca)	$Ca_{0.17}Al_{2.34}Si_{3.66}O_{10}(OH)_2$	4.24	-22.80	-39.39	-6972.63	518.12	623.45	210.72
	(Mg)	$Mg_{0.17}Al_{2.34}Si_{3.66}O_{10}(OH)_2$	4.10	-25.74	-45.66	-6920.88	502.59	611.62	204.16

Mineral		Formula	n_{CW}^*	$\Delta_{Cem.WH}$ kJ mol ⁻¹	$\Delta_{Cem.WS}$ J.mol ⁻¹ .K ⁻¹	ΔH_f^0 kJ.mol ⁻¹	S° J.mol ⁻¹ .K ⁻¹	C_p (25°C) J.mol ⁻¹ .K ⁻¹	V° cm ³ .mol ⁻¹
Vermiculite	(K)	$K_{0.86}Mg_3Si_{3.14}Al_{0.86}O_{10}(OH)_2$	3.32	-2.10	9.94	-7124.18	564.47	599.55	207.53
	(Na)	$Na_{0.86}Mg_3Si_{3.14}Al_{0.86}O_{10}(OH)_2$	3.58	-6.64	4.04	-7173.17	589.06	617.31	210.41
	(Ca)	$Ca_{0.43}Mg_3Si_{3.14}Al_{0.86}O_{10}(OH)_2$	4.12	-16.13	-14.36	-7341.81	587.92	645.94	224.25
	(Mg)	$Mg_{0.43}Mg_3Si_{3.14}Al_{0.86}O_{10}(OH)_2$	4.55	-18.89	-23.49	-7432.53	610.55	675.30	221.91

(*) n_{CW} refers to the amount of clay water per mole of hydrated clay end-member.

7. Verification of the predicting models: comparison with solubility datasets

Vieillard et al. (2019) proposed a first selection of solubility data from the literature and comparison with $\log_{10}K$ (298.15 K) estimates gives an average of $\pm 2.5 \log_{10}$ units. The selection was recently refined by Gaboreau et al. (2020) who also reported a new set of experimentally measured solubilities for clay minerals: kaolinite, smectite, illite, vermiculite and chlorite. For the latter, equilibrium was clearly not reached, even after 2 years of equilibration at 40°C. Additionally, they selected a set of solubility experiments, from previous literature. Both sets are used to assess the estimates obtained using the models described previously for the hydrated clay minerals or the anhydrous minerals for illites.

For the set of solubility data obtained by Gaboreau et al. (2020), estimates correspond to solubilities with a rather low discrepancy (max 0.37 \log_{10} units, for illite). The difference with estimates is larger for vermiculite (3.85 \log_{10} units). The Vermiculite Santa Ollala sample purified by Gailhanou et al. (2013) for the calorimetric measurements still contains an amount of impurities, like organic carbon, of which 0.42 wt. % still remains, even after H₂O₂ treatment. Such impurity, not considered in the thermodynamic cycle used to derive formation enthalpy, could affect the correctness of the extracted value. Finally and without considering chlorite solubility, the standard deviation is ± 1.3 or $\pm 0.4 \log_{10}$ units, depending whether or not calorimetry for vermiculite is considered. The average of both standard deviations, i.e. $\pm 0.9 \log_{10}$ units, produces a rather high 2σ uncertainty for $\log_{10}K$ (298.15 K) estimates ($\pm 1.7 \log_{10}$ units). This is still the most reasonable statement that can be made concerning uncertainties for $\log_{10}K$ (298.15 K) estimates in this work.

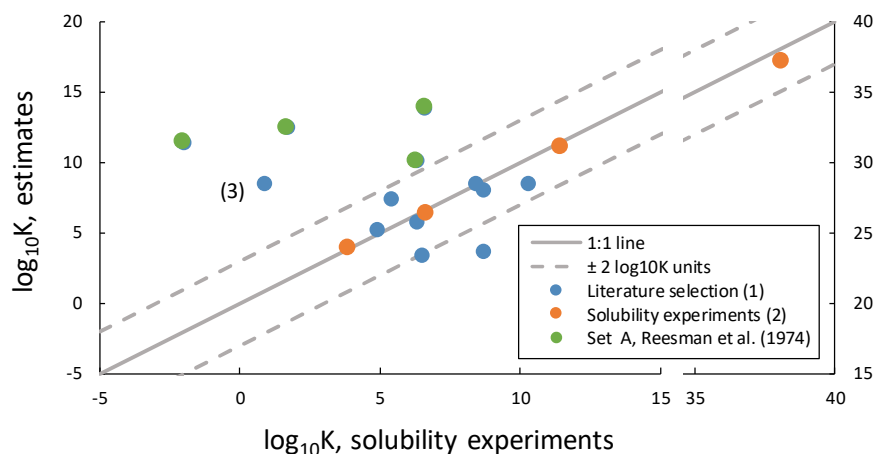


Figure 11 - Comparison between $\log_{10}K$ (298.15 K) estimates and results from previous literature studies: (1) kaolinite, smectite, illite and vermiculite from Gaboreau et al. (2020); (2) Illites and smectites from Gaboreau et al. (2020) literature selection.

As illustrated in Figure 11, predictions are in very good agreement with the solubilities measured by Gaboreau et al. (2020). The relation is still correct with the equilibrium constants extracted from literature by Gaboreau et al. (2020), providing the set of data from Reesman (1974) is discarded (set A in Figure 11). The reason for discarding this dataset could lie in the unusually high liquid/solid ratio $L/S = 200$ used by the authors, almost ten times higher than the ratio $L/S=24$ used by Misra and Upchurch (1976) and Gaboreau et al. (2020). A high L/S ratio could delay the duration required to reach equilibrium and to overestimate the stability of the mineral. The last point strongly departs from the general tendency, point (3) in Figure 2, which corresponds to the equilibrium constant extracted by Huang and Keller (1973) for the Fithian illite. It is interesting to note that the chemical composition provided by the authors strongly differs from that provided by Reesman (1974). Except for Reesman (1974) and Huang and Keller (1973) Fithian illite data, all other constants are globally located within a $\pm 2.0 \log_{10}K$ interval. This interval is close to the $\pm 1.7 \log_{10}K$ (298.15 K) previously deduced for the estimates: the estimated values are consistent with the solubility data selected from previous literature and displayed in Figure 11.

8. References

Appendix 1 - The case of illite/smectite interstratified clay minerals (I/S)

Understanding the processes associated with the transformation of smectite into illite/smectite and their consequences on the mechanical and geochemical behaviors of clayey formations is of great importance in some major application fields, such as oil exploration or nuclear waste disposal. Illite/smectite had been described as a solid solution by Aagaard and Helgeson (1983) and Garrels (1984). By collecting the chemical analyses of natural I/S samples, Meunier and Velde (1989) described the interstratified minerals using a ternary solid-solution model with one illite and two montmorillonite end-members. Based on this approach, Blanc et al. (1997) developed a thermodynamic model that allowed for the calculation of the energies of the mixing of illite and smectite layers depending on the degree of ordering of the stacking sequences.

In the framework of Thermochimie development, further advances have been realized concerning illite/smectite stability. To provide accurate constraints for such models, Gailhanou et al. (2019) have measured the thermodynamic properties of a I/S sample. The results were further interpreted using a non-ideal binary solid solution model by Blanc et al. (2021).

A1.1 - Illite/smectite calorimetric measurements

The stability of illite-smectite interstratified with respect to discrete illite and smectite minerals was investigated by measuring their thermodynamic properties. Gailhanou et al. (2019) have determined the standard thermodynamic properties (G , H , S , C_p , and V) of the illite-smectite ISCz-1 ($\text{Ca}_{0.092}\text{K}_{0.439}$)($\text{Si}_{3.562}\text{Al}_{0.438}$)($\text{Al}_{1.732}\text{Mg}_{0.255}\text{Fe}^{3+}_{0.029}\text{Fe}^{2+}_{0.011}$) $\text{O}_{10}(\text{OH})_2$ mineral, between 298.15K and 375K, by using calorimetric methods. Moreover, the enthalpies of mixing between the illite and smectite layers were measured at 298.15K by acid solution calorimetry from a complete series of illite-smectite interstratified minerals (Shinzan area, Japan). The results are given in Table A1.1.

A1.2 - Illite/smectite solid solution

Plotting ISCz-1 coordinates in a $\text{M}^+-4\text{Si}-\text{R}^{2+}$ ternary diagram (Meunier and Velde, 1989) reveals that illite-smectite ISCz-1 can be considered as a binary solid solution with a high-charge illite end-member (0.87/ $\text{O}_{10}(\text{OH})_2$), namely, IllitePP, and a low-charge montmorillonite end-member (0.21), namely, MontmorillonitePP. Their coordinates in the $\text{M}^+-4\text{Si}-\text{R}^{2+}$ diagram provide some chemical constraints. Assuming ideal mixing between elements in the illite and smectite structural sites and based on a least-square fit method allows extracting the compositions of illite and smectite end-members considering 70% illite and 30% smectite in the sample, which is consistent with the proportions obtained from the XRD analyses.

The enthalpy of mixing ΔH^{mix} can be directly obtained from the calorimetric measurements performed on the I/S series from the Shinzan area by Gailhanou (2005) and Gailhanou et al. (2019). These measurements are reported in Figure A1.1. A semi-empirical function was developed to address ΔH^{mix} variations with respect to smectite fraction X_{sm} in illite/smectite:

$$\Delta H^{\text{mix}} = x_{\text{sm}} \cdot (36.01 \cdot x_{\text{sm}} \cdot R^{2+} - 19.03) \quad \text{Eq. A1.1}$$

This function not only depends on the smectite fraction (as expected for an illite/smectite interaction term) but it also includes an octahedral composition dependence, to account for the variability observed for the Shinzan samples (Gailhanou, 2005). For comparison, the results provided using the solid solution model developed by Blanc et al. (1997) are also displayed. This model includes short range ordering and was parameterized considering diagenetic illite/smectite series. The results are similar to the measurements, at least for R1 ordered I/S samples (illite > 55 to 60 %). For the smectite-rich minerals, Blanc et al. (1997) considered that the disordered I/S stacking sequence implied $\Delta H^{\text{mix}} = 0 \text{ J. mol}^{-1}$. This statement is not correct, given the experiment results displayed in A1.1. In this work, the function from Equation (EQ. A1.1) is complemented with an ideal entropy of mixing term, to calculate the Gibbs energy of mixing.

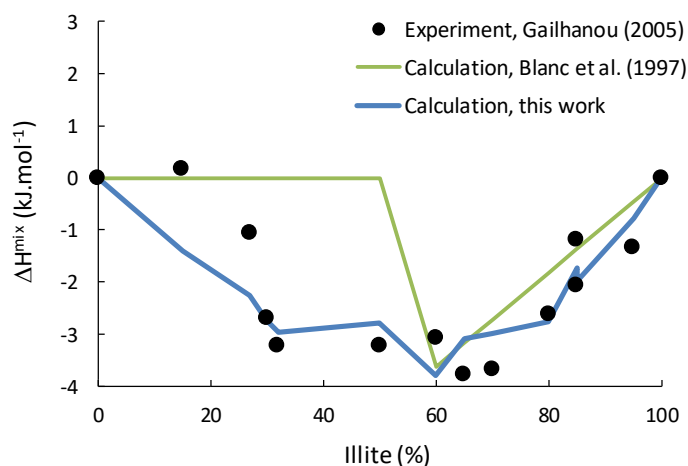


Figure A1.1 – Enthalpies of mixing determined for Shinzan series of samples from Gailhanou (2005) measurements

A1.3 - Comparison between observed and predicted values

The thermodynamic properties of illite/smectite interstratified minerals have been investigated by Blanc et al. (2021) following three distinct approaches:

- by applying the global model from Blanc et al. (2015);
- by considering a mechanical mixture of illite and smectite and applying the global model to each of the illite and smectite end-member;
- by considering a non-ideal solid solution model.

For the ISCz-1 sample, the comparison is reported in Table A1.1. From this table, the estimated $\Delta_r G^0$ is closest to the experiment values ($\Delta < 0.01 \%$) when non-ideal mixture of illite and smectite layers is considered, except for heat capacity and volume. For these latter properties, both estimate methods provide similar results and, on the whole, the method based on the solid solution improves the accuracy of the predictions for the properties of the illite-smectite ISCz-1 mineral.

Table A1.1 – Measured and estimated thermodynamic properties of ISCz-1 at 298.15 K and 101.325 kPa. $\bar{\varepsilon}_{exp}$ and $\bar{\varepsilon}_{pred}$ refers to experimental and predicted thermodynamic properties (G , H , S , C_p , V), respectively.

	ΔG_f° /kJ.mol ⁻¹	ΔH_f° /kJ.mol ⁻¹	$S^{0(tot)}$ /J.K ⁻¹ .mol ⁻¹	$C_{p,m}^\circ(298.15\text{ K})$ /J.K ⁻¹ .mol ⁻¹	V° /cm ³ .mol ⁻¹
ISCz-1 natural sample	-5418.62 ± 7.72 ^c	-5787.22 ± 7.46 ^c	295.36 ± 6.00	306.00 ± 4.59	137.13
Mean composition	-5412.63	-5779.31	301.78	317.63	137.94
$(\bar{\varepsilon}_{exp} - \bar{\varepsilon}_{pred})/ \bar{\varepsilon}_{exp} *100$	-0.11	-0.13	-2.17	-3.78	-0.59
Solid solution ^a	-5418.89	-5789.22	290.03	317.79	138.00
$(\bar{\varepsilon}_{exp} - \bar{\varepsilon}_{pred})/ \bar{\varepsilon}_{exp} *100$	0.00	0.03	1.80	-3.84	-0.63

^aillite component : $K_{0.683}Ca_{0.084}(Si_{3.319}Al_{0.681})(Al_{1.777}Mg_{0.234}Fe^{2+}_{0.016})O_{10}(OH)_2$
smectite component : $Ca_{0.107}Si_4(Al_{1.652}Mg_{0.292}Fe^{3+}_{0.081}Fe^{2+}_{0.003})O_{10}(OH)_2$

In Figure A1.2, the stability fields for the ISCz-1, Illite and Montmorillonite end-members are drawn at 25 °C by considering two different sets of thermodynamic parameters for ISCz-1:

- a set including non ideal mixing terms for the ISCz-1 properties of formation
- a set excluding non-ideal mixing terms for the ISCz-1 properties of formation.

Comparing Figures A1.2a and b highlights the importance of mixing terms. Indeed, the ISCz-1 stability field just disappears when the mixing terms are not integrated to the thermodynamic function, whereas it lies as expected between the illite and montmorillonite end-members when the mixing terms are added to the ISCz-1 formation properties.

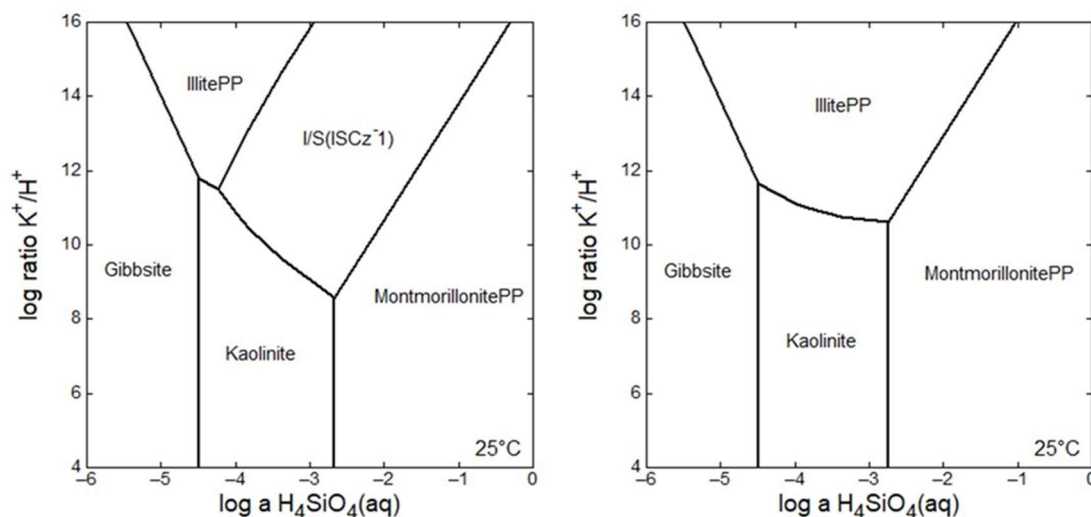


Figure A1.2 – Stability fields for the I/S ISCz-1 mineral at 298 K and ambient pressure of 101.325 kPa: a) including enthalpy of mixing and b) without enthalpy of mixing.

Overall, the most accurate calculation process to predict the thermodynamic properties of illite/smectite, implies a non-ideal, binary solid-solution model, considering a mixture of illite and smectite layers with the composition of the smectite component ranging between high- and low-charge montmorillonite, which is consistent with Meunier and Velde (1989) observations.